Solid Earth, 15, 1319–1342, 2024
https://doi.org/10.5194/se-15-1319-2024

Solid Earth Open Access EGU

On the role of trans-lithospheric faults in the long-term seismotectonic segmentation of active margins: a case study in the Andes

Gonzalo Yanez C.[1], **Jose Piquer R.**[2], **and Orlando Rivera H.**[3]

[1]Pontificia Universidad Católica de Chile, Av. Vicuña Mackenna 4860, Macul, Santiago, Chile
[2]Instituto de Ciencias de la Tierra, Universidad Austral de Chile, Valdivia, Chile
[3]Minera Peñoles de Chile, Santiago, Chile

Correspondence: Gonzalo Yanez C. (gyaneza@uc.cl)

Received: 5 May 2024 – Discussion started: 27 May 2024
Revised: 5 September 2024 – Accepted: 13 September 2024 – Published: 6 November 2024

Abstract. Plate coupling plays a fundamental role in the way in which seismic energy is released during the seismic cycle. This process includes quasi-instantaneous release during megathrust earthquakes and long-term creep. Both mechanisms can coexist in a given subduction margin, defining a seismotectonic segmentation in which seismically active segments are separated by zones where ruptures stop, classified for simplicity as asperities and barrier, respectively. The spatiotemporal stability of this segmentation has been a matter of debate in the seismological community for decades. In this regard, we explore in this paper the potential role of the interaction between geological heterogeneities in the overriding plate and fluids released from the subducting slab towards the subduction channel. As a case study, we take the convergence between the Nazca and South American plates between 18–40° S, given its relatively simple convergence style and the availability of a high-quality instrumental and historical record. We postulate that trans-lithospheric faults striking at a high angle with respect to the trench behave as large fluid sinks that create the appropriate conditions for the development of barriers and promote the growth of highly coupled asperity domains in their periphery. We tested this hypothesis against key short- and long-term observations in the study area (seismological, geodetic, and geological), obtaining consistent results. If the spatial distribution of asperities is controlled by the geology of the overriding plate, seismic risk assessment could be established with better confidence.

1 Introduction

Subduction margins accommodate short-term (years to tens of years) and long-term (thousands to millions of years) deformation. The most evident effects of these two deformational behaviours are earthquakes (short-term) and mountain-building (long-term) (e.g. Avouac, 2007). The concept of the seismic cycle, introduced by Fedotov (1968) and further elaborated by Mogi (1985), identifies two stages: a long inter-seismic period (several tens of years) followed by a short co-seismic period (minutes at most), where the elastic energy stored during the previous stage is released as an earthquake. For earthquake magnitudes in the range of M_w 7.5–9.5, the observed mean slip displacement varies from 0.8–10 m (Thingbaijam et al., 2017). Even though the maximum mean slip in megathrust events is 10 m, the zones of maximum slip, equated to asperities (e.g. Aki, 1984; Lay and Bilek, 2007; Lay, 2015) can reach 20–40 m in wavelength patches in the range of 20–100 km (see, e.g. http://equake-rc.info/srcmod/, last access: 13 February 2024). However, the release of elastic energy during the seismic cycle only accounts for 90 %–95 % of the deformation accumulated interseismically in convergent margins; the remaining 5 %–10 % produces permanent deformation in the overriding plate, expressed as crustal shortening and mountain-building (e.g. Yañez and Cembrano, 2004). This long-term process lasts for hundreds to thousands of seismic cycles (time windows of millions of years). Therefore, both phenomena – earthquakes and mountain-building – are extreme

responses to the same process, namely the convergence between oceanic and continental plates.

The concepts of asperities and barriers were proposed by Lay et al. (1982) and Aki (1984) to describe the process during the occurrence of an earthquake and intimately related to the concept of plate coupling. More recent studies (e.g. Bilek and Lay, 2007) propose a more complex mechanism at the subduction plate contact in which domains of unstable stick-slip states coexist with other domains in a conditionally stable stick-slip state and zones that develop aseismic slip/stable behaviour. These three states – unstable, conditionally stable, and stable stick-slip behaviour – represent different slip modes that can be represented as asperities and barriers in the old nomenclature (Scholz, 1990). However, the conceptualisation of Bileck and Lay (2007) proposes a down-dip (depth) distribution of the different slip behaviours, namely (1) aseismic-stable at depths of 5–10 km, (2) mostly conditionally stable at depths of 10–15 km, and (3) unstable stick-slip behaviour (Brace and Byerlee, 1966; Burridge and Knopoff, 1967) at depths of 15–25 km. Recent studies on exhumed subduction domains in California (Platt et al., 2018) corroborate this down-dip transition from seismic zone to transition zone. One interesting characteristic of these domains is that unstable domains are generally surrounded by conditionally stable domains and aseismic domains in their outermost periphery.

To date, there is no clear evidence on whether the geological/tectonic process(es) control to some extent these seismogenic behaviours and/or their stability across several seismic cycles or geological time frames. Potential candidates already proposed include (1) the roughness of the subducting plate (aseismic ridges, fracture zones, horst/graben structures, etc.) (e.g. Bilek et al., 2003; Wang and Bilek, 2011; Geersen et al., 2015; Philibosian and Meltzner, 2020; Molina et al., 2021); (2) fluid-controlled overpressure (Peacock, 1993; Saffer and Tobin, 2011; Saffer, 2017; Menant et al., 2020); (3) the shape of the subducting plate (e.g. Gutscher et al., 1999); and (4) the geology of the overriding plate (i.e. Kimura et al., 2018; Philibosian and Meltzner, 2020; Molina et al., 2021), among others, including various combinations of these different possible factors.

The role of fluids released from the subducting slab has emerged as a first-order factor in the plate-coupling processes at subduction margins. Direct observations (e.g. Saffer and Tobin, 2011; Tsuji et al., 2014; Moreno et al., 2014) and numerical modelling (Menant et al., 2020) demonstrate that fluids released from the subducting oceanic crust and subduction channel define segments at the plate-coupling zone with distinct pore pressure characteristics. Overpressure domains are associated with zones of weak coupling, and strong coupling is observed in the case of zones showing low-pore-pressure behaviour. The first type of domain is in direct association with creep zones or slow-slip events, while the other one is in direct association with locked zones or, in the seismological nomenclature, the barrier and asperity domains, respectively. Seismic imaging of the forearc wedge (e.g. Tsuji et al., 2014) and numerical modelling also show that fluids percolate upwards in the zones of maximum overpressure, including the emplacement of serpentinite bodies along weak zones or faults.

In this paper, we propose a causal relationship between the presence of trans-lithospheric faults (TLFs) in the overriding plate and seismic segmentation, involving the control of TLFs on the movement, storage, or release of overpressure fluids along and across the subduction zone. We use the central southern Andes as a case study, as it is one of the most active seismogenic sites worldwide, is well studied, and has a relatively simple subduction geometry (Hayes, 2018). In addition, recent structural and geophysical mapping has revealed the role of TLFs in the tectonomagmatic evolution of the continental margin of this region (e.g. Yañez et al., 1988; Santibáñez et al., 2019; Cembrano and Lara, 2009; Melnick and Echtler, 2006; Yañez and Rivera, 2019; Piquer et al., 2019, 2021a). We aim to demonstrate that the interaction between these TLFs and the fluid circulating through the subduction channel provides a simple first-order explanation for the Andean seismotectonic organisation through a long-lived geological control.

2 Data and methods

2.1 Tectonic background

The Nazca–South American plate convergence is a subduction-type margin that has been active in this segment of the Andes since at least the Cretaceous without the accretion of new terrains (Mpodozis and Ramos, 1990). Since 15 Ma, the convergence has been slightly oblique (E10° N) at a velocity of around 6.5 cm yr^{-1} (Angermann et al., 1999). The age of the oceanic plate varies between 0 Ma at the triple junction of Taitao (44° S) to 45 Ma at the orocline bending of Bolivia (18° S) (Fig. 1). A flat slab segment is located between 28° S and 33° S latitude, affecting the development of an asthenospheric wedge landward and inhibiting the occurrence of active volcanism since the last 5 Myr (Kay and Mpodozis, 2002). However, the Wadati–Benioff plane is roughly homogenous in dip along the plate boundary between the Nazca and South American plates (Slab 2.0, Hayes, 2018). The roughness of the Nazca Plate is affected by a progressively older oceanic crust northward, with some fracture zones offsetting the plate, the subduction of a triple junction with an active spreading centre (now at Taitao Peninsula), some episodic magmatic activity along the Juan Fernández Ridge (33° S; Yáñez et al., 2001), and eventually a smaller ridge at 20° S (Perdida ridge; Cahill and Isacks, 1992). Overall, these features can be described as minor obstacles to the subduction of a relatively young oceanic plate underneath a continental plate in a highly coupled convergent margin (Sect. 2.5).

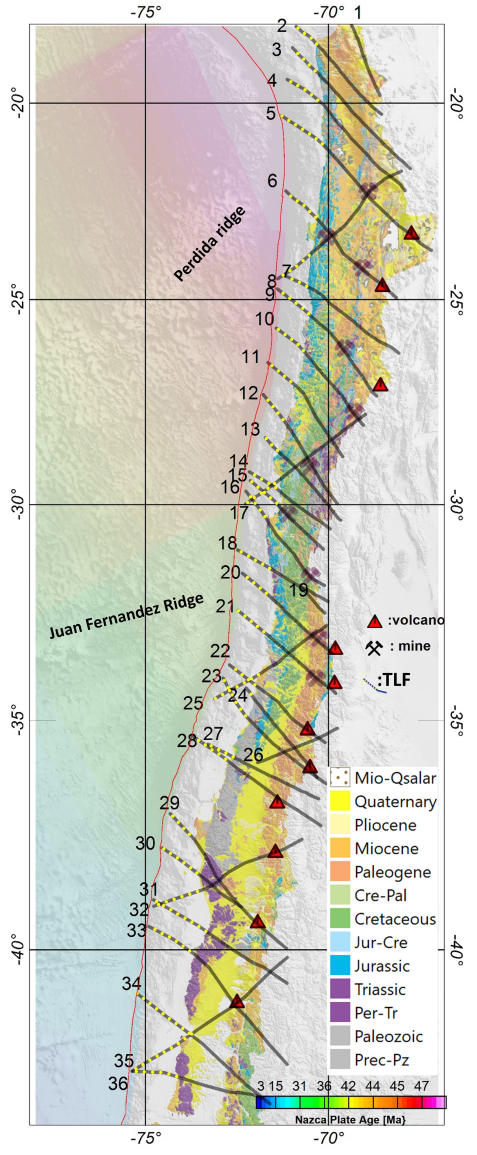

Figure 1. The spatial distribution of trans-lithospheric faults (TLFs) over the regional geology of the Chilean continental margin (from SERNAGEOMIN, 2003). The traces of the TLFs are based on the models of Yáñez and Rivera (2019) and Piquer et al. (2019) in northern and central Chile and follow the model of Melnick and Echtler (2006) in southern Chile. Also shown are the locations of the main ore deposits (from north to south, Chuquicamata, Mantos Blancos, Escondida, Salvador, Cerro Casale, El Indio, Andacollo, Los Pelambres, Río Blanco–Los Bronces, and El Teniente) and active volcanoes (from north to south, Láscar, Llullaillaco, Ojos del Salado, Tupungatito, Maipo, Planchón-Peteroa, Laguna del Maule, Chillán, Callaqui, Villarrica, and Osorno) to show their correspondence with the TLF array. TLFs are extended until the trench, following their main trend, and the canyons trace to the south of 36° S, using segmented red lines to highlight the uncertainty in this offshore extension. In the seaward side of the figure, the age map of Müller et al. (2019) is included with the bathymetry of the seafloor.

2.2 Compilation of trans-lithospheric faults in the Andean active margin and their role as long-lived high-permeability domains

Trans-lithospheric faults (TLFs) correspond to long-lived, high-angle fault systems which have been identified in several segments of the Andean margin, based on geological mapping (e.g. Santibañez et al., 2019; Cembrano and Lara, 2009; Melnick and Echtler, 2006; Piquer et al., 2021a; Farrar et al., 2023; Wiemer et al., 2023), crustal seismicity (e.g. Talwani, 2014), a combination of indirect geophysical techniques (Yañez et al., 1998), or a combination of all of these (Yañez and Rivera, 2019; Piquer et al., 2019; Pearce et al., 2020). The geometry and depth extension of TLFs is unknown, but based on their control of the continental-scale magmatic and hydrothermal processes and their surface traces of the order of hundreds of kilometres, we consider that they involve, exclusively, the whole lithosphere.

In Table 1 we present a synthesis of the current status of knowledge regarding TLF definitions and the major geological/geophysical evidence that described them. The number assigned in each case is used later on in Fig. 1 as an identifier.

Detailed structural mapping in various segments of the Andean margin has provided direct geological evidence of the presence of TLFs. They are manifested in the field as networks of individual high-angle faults, defining deformation zones with widths of up to several kilometres and lengths of the order of hundreds of kilometres, making it possible to follow their trace across the entire continental margin (Lanza et al., 2013; Yáñez and Rivera, 2019; Piquer et al., 2021a). These fault networks correspond to the expression at the present-day surface of a pre-existing TLF, as a result of its vertical propagation through Mesozoic and Cenozoic igneous and sedimentary rocks (McCuaig and Hronsky, 2014; Piquer et al., 2019). Field observations also show that, consistent with their high dip angle (commonly $> 60°$ and in several cases a sub-vertical angle, although individual fault segments can dip at slightly lower angles), TLFs tend to be reactivated as basin-bounding faults during extensional episodes and are thus associated with sharp changes in the stratigraphic record (Piquer et al., 2015, 2021a; Yáñez and Rivera, 2019). They also control the distribution of exhumed basement blocks (Yáñez and Rivera, 2019).

The geological record demonstrates that TLFs are long-lived structures that have played a major role in the long-term evolution of the Chilean continental margin and are reactivated with different kinematics under varying tectonic regimes. It is likely that several TLFs originated in the Proterozoic and the Palaeozoic (Yáñez and Rivera, 2019); there is strong geological evidence suggesting the present-day TLF architecture was already in place by the Permo-Triassic, a period in which these structures acted as master and transfer faults for intra-continental rift systems (Niemeyer et al., 2004; Sagripanti et al., 2014; Espinoza et al., 2019). Syn-

Table 1. Main trans-lithospheric faults of the Chilean Andes (17–42° S latitude).

LSS_ID	LSS_NAME	References	Geological evidence
1	Visviri	(15), (22)	(L)(TLS)(SC)(GVA), Antofalla Basement (T)
2	Arica	(15), (21), (22)	Arequipa Massif (T), ETL NW Arica (TLS)
3	Camarones	(22)	(TLS)(GVA)(SDGU)
4	Iquique	(22)	(TLS)(GVA)(SDGU)
5	Calama	(1), (2), (8), (20), (21), (22), (24)	Comache (F), Calama–Olacapato–El Toro (L)(FS)(VA), Solá (F), Chorrillos (F), ETL NW Calama (TLS)
6	Mejillones–Llullaillaco	(8), (10), (21), (22), (29), (35)	Archibarca (L)(VA), Cataclasitas de Sierra de Varas (DZ), ETL NW Mejillones (TLS), Socompa (FS)
7	Agua Verde–Exploradora	(8), (22)	Culampajá (L)
8	Antofagasta–Conchi	(22), (27), (28), (30)	Antofagasta–Calama (L)(PMG)(TR)(STMH)
9	Taltal–Potrerillos	(8), (22)	Taltal (L)(TLS)(SDGU)(VA)(STMH)
10	Chañaral	(8), (22)	(TLS)(GVA)(SDGU)
11	Copiapó	(22)	(TLS)(SDGU)
12	Vallenar	(22)	(TLS)(SDGU)
13	Domeyko	(22), (36)	(TLS)(GVA)(SDGU), Cruzadero (F)
14	Vicuña	(22)	(TLS)(GVA)(SDGU)
15	Andacollo	(22)	(TLS)(GVA)(SDGU)(STMH)
16	Punitaqui–Los Pelambres	(22)	(TLS)(GVA)(SDGU)(MA)(STMH)
17	El Potro	(22)	(TLS)(SDGU)
18	Illapel	(22)	(TLS)(GVA)(SDGU)
19	Almendrillo	(22)	(TLS)(GVA)(SDGU)
20	La Ligua–Los Andes	(21), (22), (31)	(TLS)(GVA)(SDGU)(SC)(MA), Río Blanco–Los Bronces (FS)(STMH)
21	Valparaíso–Volcán Maipo	(3), (5), (7), (19), (21), (22), (23), (26)	Piuquencillo (F)(FS)(STMH), Melipilla (F)(MA), Marga Marga (FS), Valparaíso–Curacaví (FS)(STMH), Concón (MDS), Cartagena (MDS), El Tabo (MDS)
22	Pichilemu	(9), (17), (22), (23), (24), (25)	Pichilemu (ATS), Teno (FS)(SC)(STMH), Planchón-Peteroa (LLBS)(SC)
23	Laguna del Maule	(32), (33)	Río Maule (F)(VA)(SDGU)(STMH)
24	Iloca–Rio Melado	(34)	Laguna Fea (FS)(VA)(STMH)
25	Aconcagua–San Antonio	(4), (6), (22), (23), (31)	Puangue (F), Estero Chacabuco (F), Estero Colina (F), El Salto (FS)(STMH)
26	Volcán Quizapu	(33)	(VA)(MDS)
27	Parral–Bullileo	This study	(VA)(SDGU)
28	San Carlos–Nevados de Chillán	(12), (17), (18)	Chillán (AZ), Nevados de Chillán–Tromen (LLBS), Cortaderas (L)
29	Lanalhue–Volcán Villarrica	(11), (14), (16), (17), (24)	Morguilla (FLS), Lanalhue (F)(FS), Villarrica–Quetrupillán–Lanín (LLBS)
30	Tirúa–Pitrufquén	(11), (16)	Mocha–Villarrica (FS)

Table 1. Continued.

LSS_ID	LSS_NAME	References	Geological evidence
31	Rio Calle-Calle–Lago Ranco	(13), (17)	Carrán–Los Venados (LLBS), Futrono (F)
32	Puerto Saavedra–Volcán Callaqui	(18)	Copahue–Callaqui (AZ)
33	Osorno–Volcán Calbuco	This study	(VA)
34	Ancud–Volcán Michimahuida	(17)	Michimahuida (LLBS)
35	Cucao–Chaitén	(17)	Chaitén (LLBS)
36	Chacao–Osorno–Puntiagudo	(17)	(VA)

ATS is for Andean transverse system; AZ is for accommodation zone; DZ is for deformation zone; F is for fault; FLS is for fault line scarp; FS is for fault system; GVA is for gravimetric anomaly; L is for lineament; LLBS is for long-lived basement structure; MA is for magnetic anomaly; MDS is for mafic dike swarm; PMG is for palaeomagnetism; SC is for seismic cluster; SDGU is for structural discontinuity of geological unit; T is for terrane; TLS is for trans-lithospheric structure; TR is for tectonic rotation; STMH is for syn-tectonic magmatic–hydrothermal centre; VA is for volcano alignment.
(1) Salfity, 1985; (2) Marrett et al., 1994; (3) Gana et al., 1996; (4) Wall et al., 1996; (5) Yáñez et al., 1998; (6) Wall et al., 1999; (7) Rivera and Cembrano, 2000; (8) Chernicoff et al., 2002; (9) Sernageomin, 2003; (10) Niemeyer et al., 2004; (11) Haberland et al., 2006; (12) Ramos and Kay, 2006; (13) Lara et al., 2006; (14) Glodny et al., 2008; (15) Ramos, 2008; (16) Melnick et al., 2009; (17) Cembrano and Lara, 2009; (18) Radic, 2010; (19) Creixell et al., 2011; (20) Lanza et al., 2013; (21) Rivera, 2017; (22) Yáñez and Rivera, 2019; (23) Piquer et al., 2019; (24) Santibáñez et al., 2019; (25) Pearce et al., 2020; (26) Piquer et al., 2021a; (27) Arriagada et al., 2003; (28) Peña, 2022; (29) Richards et al., 2013; (30) Palacios et al., 2007; (31) Piquer et al., 2015; (32) Kohler, 2016; (33) Fischer, 2021; (34) Torres, 2021; (35) Farrar et al., 2023; (36) Giambiagi et al., 2017.

tectonic emplacement of magma along TLFs has been documented at least since the Jurassic (Creixell et al., 2011).

Geophysical support for the TLF architecture in the continental margin is provided by the geometry of magnetic and gravimetric anomalies (Piquer et al., 2019; Yáñez and Rivera, 2019) and also by magnetotelluric data (Pearce et al., 2020) and seismic tomography (Yáñez and Rivera, 2019). Evidence of seismic activity in some of these TLFs has been recorded, for example, a precursory event to the 9.3 M_w 1960 Valdivia earthquake (Lanalhue fault; Melnick et al., 2009) and the coseismic rebound associated with the 8.8 M_w 2010 Maule earthquake (Pichilemu Fault; e.g. Farías et al., 2011; Aron et al., 2013). Additionally, researchers have documented a strong spatial relationship between a TLF and a major seismic swarm (Valparaíso seismic sequence of 2017; Nealy et al., 2017) at the subduction megathrust (Piquer et al., 2021a).

Regarding the role of TLFs as long-lived high-permeability domains, Yañez and Rivera (2019) postulated that they represent weak lithospheric domains that favour fluid flow and the emplacement of different types of ore deposits over large time periods (tens of millions of years), beginning with stratabound and iron oxide–copper–gold (IOCG)-type deposits in the Jurassic. A similar conclusion has been reached by Farrar et al. (2023) for the emplacement of porphyry copper deposits of various ages and by Wiemer et al. (2023) for gold-rich superclusters of various types of mineral deposits. The strong relationship between the locations of TLFs and those of giant ore deposits at specific metallogenic belts has been discussed more specifically in the Andes of northern (e.g. Chernicoff et al., 2002) and central Chile (e.g. Piquer et al., 2016) and neighbouring regions in Argentina. Similarly, there is a well-established relationship between the locations of TLFs and volcanic/geothermal activity in the Andes of southern Chile (e.g. Cembrano and Lara, 2009). Moreover, high Vp/Vs ratios that were documented during the Pichilemu seismic sequence following the 2010 Maule earthquake have been interpreted as strong evidence of fluid migration (Farías et al., 2011; Calle-Gardella et al., 2021).

Various authors have discussed how the type of magmatic–hydrothermal product and fluid flow regime varies depending on the orientation of a specific high-angle fault system (in several cases, a TLF) relative to the predominant stress tensor (Lara et al., 2006; Cembrano and Lara, 2009; Roquer et al., 2017; Piquer et al., 2021b). Of particular relevance is the orientation of the fault system relative to the maximum stress ($\sigma 1$); if the fault system is sub-parallel or strikes at a low angle relative to $\sigma 1$, it is well-oriented for opening and reactivation, respectively, allowing the rapid ascent of magma and hydrothermal fluids through different crustal segments. On the other hand, if the fault system is sub-perpendicular or strikes at a high angle relative to $\sigma 1$, it would be poorly oriented or misoriented for reactivation and would promote the storage of magma and hydrothermal fluids at depth (e.g. Cembrano and Lara, 2009; Stanton-Yonge et al., 2016; Piquer et al., 2021b). In the latter case, a requirement for fault reactivation and the release of the accumulated fluids is that supra-lithostatic fluid pressures are achieved; once this occurs, the fault system would allow the discharge of the accumulated fluids towards upper crustal levels and would act as a fluid pump ("fault–valve behaviour"), concentrating fluids in the fractured areas within the fault system and leading to the depletion of fluids in the surrounding regions (Sibson, 1990, 2020; Cox, 2016). These fluid discharge events cause seismic swarms (Cox, 2016), which concentrate at the base of the high-angle fault system (Sibson, 2020).

Figure 1 presents the main array of NW- and NE-striking TLFs observed in the Andean margin; their seaward trend has been extrapolated following the observed trend in the continental lithosphere, in particular south of 36° S, following the trace of submarine canyons.

2.3 Historic subduction seismicity and slip solutions during the last 50 years and trans-lithospheric fault (TLF) correspondence

The historic seismic record in the region is short, extending from the start of the Spanish colonisation in the region (present territories of Peru and Chile, circa 1500). Compilations of historic seismicity and subsequent interpretation to assess the magnitude and longitudinal extension of the events have been provided in Ruiz and Madariaga (2018) and Scholz and Campos (2012), among others. Figure 2a includes all the historic events described by these authors, as well as events above 7 M_w from the USGS (United States Geological Survey) catalogue. As noted by several authors (Ruiz and Madariaga, 2018, and references therein), there is evidence of seismotectonic segmentation in the historic record. For the present analysis, we define seven domains from north to south; the boundary between domains is defined by a region of roughly 100–200 km that represents the uncertainty in the rupture length of the major events. We consider wider boundaries for the cases lacking information, in particular in the northern area where the historic record is sparse. Domain I, in the northernmost part of the study region, shows a sequence of events close to magnitude 8 M_w and separated by 100–150 years. Domain II has no large events (above 8 M_w) in the historic record, instead having a series of intermediate events of magnitude 7–7.7 M_w between 1960 and 2020. Domain III has two events with magnitudes in the range 8.3–8.5 M_w separated by almost 10 years but with a current seismic gap of 100 years. Domain IV is shorter than 200 km in length and includes a series of seismic events of magnitude 8 M_w or above. According to Ruiz and Madariaga (2018), the three major events in this domain show relatively consistent recurrence times (60–80 years) and magnitudes (8–8.4 M_w), i.e. the earthquakes of 2015 (Illapel; 8.3 M_w), 1943, and 1880. Domain V is also relatively small, about 300 km, and includes regular events of around 8 M_w, including the Valparaíso 1985 8 M_w event and the 1906 8.4 M_w event. Domains VI, VII, and VIII include part of the Maule 2010 8.8 M_w and Concepción 1835 8.6 M_w events but are defined as such based on some events that had less than 8 M_w. Domain X, the southernmost domain, is dominated by the giant events of Valdivia 1960, 9.5 M_w, and 1737, 9.0 M_w.

Adequate seismic coverage is available since 1985 in Chile. In this period, six large earthquakes have been recorded, namely Valparaíso 1985, 8.0 M_w (Comte et al., 1986; Mendoza et al., 1994); Antofagasta 1995, 8.0 M_w (Ruegg et al., 1996; Delouis et al., 1997; Pritchard et al., 2002; Chlieh et al., 2004); Tocopilla 2007, 7.8 M_w (Schurr et al., 2012); Maule 2010, 8.8 M_w (Delouis et al., 2010; Lay et al., 2010; Vigny et al., 2011; Koper et al., 2012; Ruiz et al., 2012; Moreno et al., 2012; Lorito et al., 2011; Lin et al., 2013; Yue et al., 2014); Iquique 2014, 8.2 M_w (Ruiz et al., 2014; Hayes et al., 2014; Schurr et al., 2014; Lay et al., 2014), and Illapel 2015, 8.3 M_w (Melgar et al., 2016; Heidarzadeh et al., 2016; Li et al., 2016; Lee et al., 2016; Satake and Heidarzadeh, 2017). Given the large size of the Valdivia 1960 earthquake (9.5 M_w), we also include slip estimates for this event based on surface deformation data (Barrientos and Ward, 1990). The slip distribution of these events ranges from 1 m (e.g. Tocopilla 2007 and Antofagasta 1995) to several metres (e.g. Illapel 2015 and Iquique 2014) and more than 10 m (Valdivia 1960 and Maule 2010); however, in Fig. 2b, we normalise the slip distribution with respect to the corresponding maximum slip in each case, plotting over the slab surface to highlight its spatial distribution. This approach aims to highlight the zones of maximum slip in each case and to appreciate their spatial and temporal distribution under the working hypothesis that they represent the zones of maximum slip and are most likely a good proxy to identify asperities in the plate contact zone. These maximum slip zones are generally distributed between the TLF network (Fig. 2).

2.4 Cumulative seismic spatial distribution in the last 20 years

The seismic activity, apart from its spatiotemporal distribution around megathrust events (occasionally with foreshocks and normally with a hyperbolic distribution of aftershocks in time; Omori's law), shows some clustering (denominated in general as seismic swarms), which may be triggered by aseismic creep events (Forsyth et al., 2003; Roland and McGuire, 2009) associated with the presence of fluids in the fault zone. In the Andean plate convergence margin, recent studies also show examples of seismic swarm distribution attributable to fluid pore pressure processes (e.g. Poli et al., 2017; Pasten-Araya et al., 2018). To contextualise the spatial distribution of this seismicity, we compute a normalised seismic density distribution along the margin for the last 20 years in which the seismic network is complete above magnitude 3 M_w. We exclude most of the seismicity associated with major thrust events in this period, filtering out the events at distances shorter than 200 km from the rupture zone in a temporal window of 200 d. We acknowledge that this 20-year time window is too short to obtain a broad and complete picture of the distribution of swarms along the margin. However, as swarms normally last for just a few weeks or 1–2 months at most, the cases observed in this time window provide insights into their spatial distribution. The data used in this analysis were obtained from the database of the National Seismological Centre (CSN in Spanish). We selected data attributable to the seismogenic plate contact within a 10 km thick volume, following the slab 2.0 Wadati–Benioff plane (Hayes, 2018).

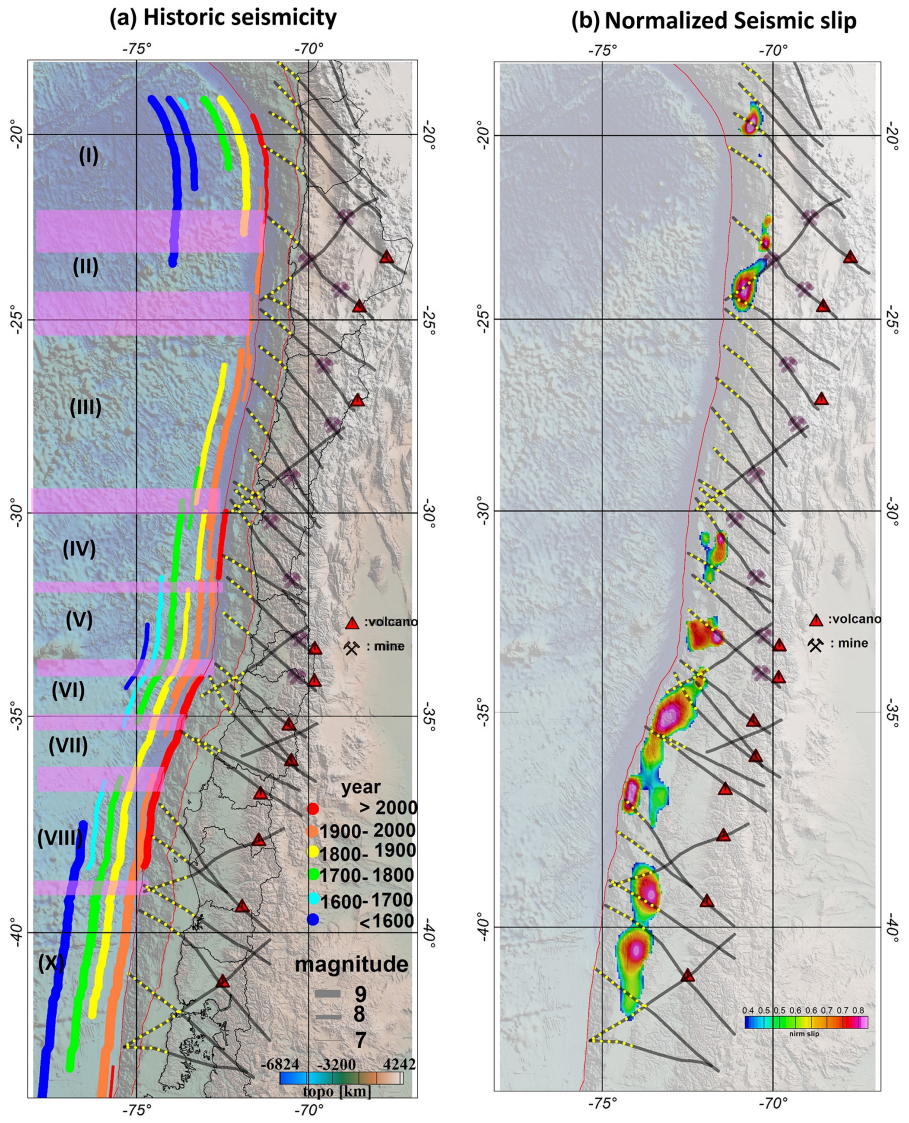

Figure 2. Panel **(a)** shows historical seismicity from the years 1450 to 2020 (HIS) (for a full description of each event, see Table S1 in the Supplement). The lateral extent of each event indicates the north–south estimate of the event name; the colour scale corresponds to the year window of each event; the M_w magnitude is represented by the width of the line. Seismotectonic segmentation is indicated by pink semi-transparent ribbons, which are extended downwards to the lower panels. Panel **(b)** shows zones of maximum slip in the megathrust events registered at the margin of Chile since 1960; the colour code represents a normalised slip to the maximum slip in each event (SLIP).

The seismic density distribution is shown in Fig. 3a; we can see that seismicity tends to cluster in the vicinity of the seaward projection of the TLFs.

2.5 Distance from the trench to the shelf brake

Saillard et al. (2017) show that peninsulas along subduction zone coastlines present a long-term permanent coastal uplift that can be associated with creep and aseismic slip domains. Thus, the distance from the trench to the coast (DTC) constitutes a proxy to separate seismotectonic segmentation due to the weak plate coupling. The physics behind this proposal lies in the dragging force that subduction force induces on the overriding plate, thus with less traction (weak plate coupling in the long term), the forearc region close to the trench should be shallower than the surroundings. To gain a broader perspective of the peninsula's distribution, Fig. 3b contours the distance to the shelf brake, which is probably a better proxy for a potential uplifted domain in the coastal region. As shown in this figure, the DTC presents variations along the trench. We identify domains of a short DTC associated with peninsulas in the region near to Arauco, Valparaíso, Tongoy, Punta de Choros, and Mejillones. Based on geological and geochronological evidence in three of these peninsulas (Mejillones, Tongoy, and Arauco), Saillard et al.

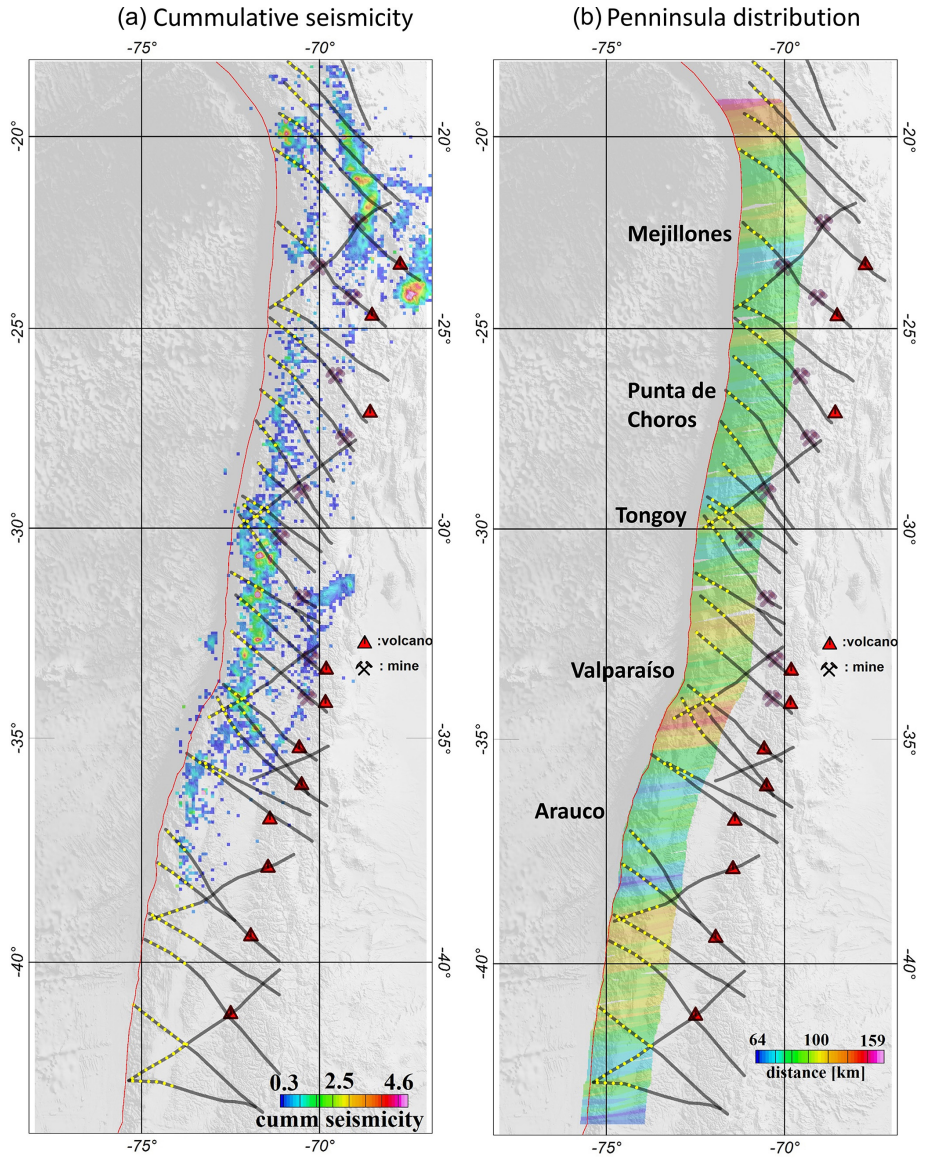

Figure 3. (a) Density distribution of the last 20 years of seismicity in the margin (CUMM) (data from National Seismological Centre, CSN); values are normalised to better define the zones where seismicity has been concentrated, filtering out all the aftershocks associated with major megathrust activity (Taltal 2001, Maule 2010, Iquique 2014, and Illapel 2015). **(b)** Distance from the trench to the shelf brake projected to the convergence direction 10° E (DIST).

(2017) determined uplift rates in the range of 0.6–2 m per 1000 years in the associated terraces. These terraces have been continuously uplifting for at least the last 0.5–0.8 Myr, indicating a long-term process compared to the seismic cycle of less than 500 years. Using this evidence, in addition to the inter-seismic GPS coupling, Saillard et al. (2016) infer that these peninsula zones are associated with weak plate coupling, where deformation is mostly accommodated by creep. Again, qualitatively speaking, there is a tendency to find peninsula distribution where TLFs tend to concentrate in the coastal region.

2.6 Viscous coupling

The negative free-air anomaly along the Chile–Peru Trench is the response to dynamic equilibrium between buoyancy and tectonic forces (Yáñez and Cembrano, 2004). The tectonic force tends to drag the continental plate downwards, whereas buoyancy restores this deformation. Assuming equilibrium between the net tectonic force and the long-term deformation (flow in continuum physics), the observed bathymetry represents this force equilibrium. Therefore, for each bathymetric observation, a given slip layer viscosity (SLV) (Wdowinski, 1992) allows a match between obser-

vations and long-term viscous plate coupling. Using the methodology developed by Yáñez and Cembrano (2004), we determine the along-strike SLV in the Nazca–South America plate convergence region, considering across-strike profiles every 20 km. As indicated earlier, zones of maximum slip involve wavelengths larger than 20 km for the megathrust events, and therefore, a sample interval of 20 km ensures an appropriate along-strike resolution. In addition, following the same rationale and conclusions of Yáñez and Cembrano (2004), we estimate that the increase in the SLV in the north of the study area is due to a temperature-dependent rheology. This increase in viscous plate coupling in the north is likely to be responsible for the larger crustal shortening observed in the southern Andes in the last 20 Myr. Although other authors (e.g. Lamb and Davis, 2003) consider that the deficiency in sedimentary supply in the trench in the northern Andes is the driving mechanism for the larger viscous plate coupling in the region. However, this discussion is beyond the scope of the present work, and since the viscous plate coupling correctly represents the observations, we are interested here in the short-wavelength viscous plate response as a potential tool to identify zones with different degrees of coupling along the convergent margin. Therefore, we remove this regional viscous plate coupling to isolate short-wavelength features. This residual slip layer viscosity (RSLV) is included in Fig. 4a (see a full discussion in Sect. S1 in the Supplement). This signal shows positive (high relative viscous plate coupling) and negative (weak relative coupling) zones. Again, we use normalised values to highlight the spatial distribution of the signal. In the Supplement, we present a full description of the modelling used to obtain the RSLV signal. As the modelling is 1D, we extend the result of each model along the strike of the convergence (10° E).

2.7 Inter-seismic GPS coupling

GPS data provide information on the surface deformation relative to a stable continental reference. During the inter-seismic period, the slip velocity at the intraplate contact, Vinter-seismic, can be determined from a GPS network under the assumption of elastic plate deformation (e.g. Okada, 1985). This inter-seismic velocity depends on the degree of plate coupling, Φ. At maximum plate coupling ($\Phi = 1$), Vinter-seismic is null, and at minimum plate coupling ($\Phi = 0$), Vinter-seismic is equal to the convergence velocity (Vconvergence). Or, mathematically (e.g. Metois et al., 2012), Vinter-seismic $= (1 - \Phi) \cdot$ Vconvergence. Inter-seismic GPS coupling is presented as GPS-locking data in Fig. 4b (based in a compilation of GPS information derived from different sources; Burgmann et al., 2005; Chlieh et al., 2008; Loveless and Meade, 2011; McCaffrey et al., 2002; Metois et al., 2012, 2016; Moreno et al., 2010, 2012; Wallace et al., 2004). For the segment between Antofagasta and Copiapó (24–28° S), two new GPS plate-coupling models are available (Yáñez-Cuadra et al., 2022, and González-Vidal et al., 2023); however, we noticed that these new results share similarities that do not depart significantly from the model presented in Fig. 4b and are thus are not included in this case. From 27° S to the north, high GPS plate coupling is generally observed, although some correspondence is observed with the local minimum and TLF distribution. Between 27–33° S, the GPS coupling shows domains with lower values with better correspondence with TLF segmentation and the minimum in viscous coupling. To the south of 33° S, the GPS plate coupling not only shows a spatial distribution that again shows some coincidence with the other proxies but also some discrepancies. This is not surprising, since GPS inter-seismic plate coupling reflects the quasi-instantaneous coupling of seismotectonic segments at different loading stages. Nevertheless, in most of the studied segments, the GPS plate coupling correlates relatively well with the viscous plate coupling, and the location of peninsulas and cumulative seismicity in the last 20 years.

3 Discussion

3.1 Quantitative correlation between TLFs and plate-coupling proxies derived from seismicity distribution, GPS and viscous coupling, and coastal morphology

In order to better quantify the correspondence between the spatial distribution of TLFs and the indirect estimate of plate coupling described in Sect. 2, we present here an objective comparison between them. This task is challenging and requires taking into consideration the poorly constrained data used. (a) In some cases, the data include regional-scale geological observations (TLFs and peninsula distribution); (b) different timescale coupling estimates (inter seismic GPS locking and long-term viscous coupling); (c) poorly resolved GPS solution offshore; (d) 1D modelling of viscous coupling; and (e) the lack of completeness in the seismicity record (historical record of 500 years, instrumental record of megathrust events of 50 years, and cumulative seismicity of 20 years), considering a seismic cycle of a couple of hundred years in the margin. Thus, no single independent proxy is capable of producing a reliable estimate by itself but rather a combination of them. Therefore, a thorough analysis is beyond the capabilities of the data source, and what we present here, though quantitative, should be understood as a guide to determine tendencies from different and independent perspectives that, as a whole, provide a more robust estimate on the link between TLFs and plate coupling in the margin.

The approach adopted considered the spatial correlation between TLFs and the six proxies described in Sect. 3, using the Pearson correlation coefficient between two variables (r_{xy}) defined as

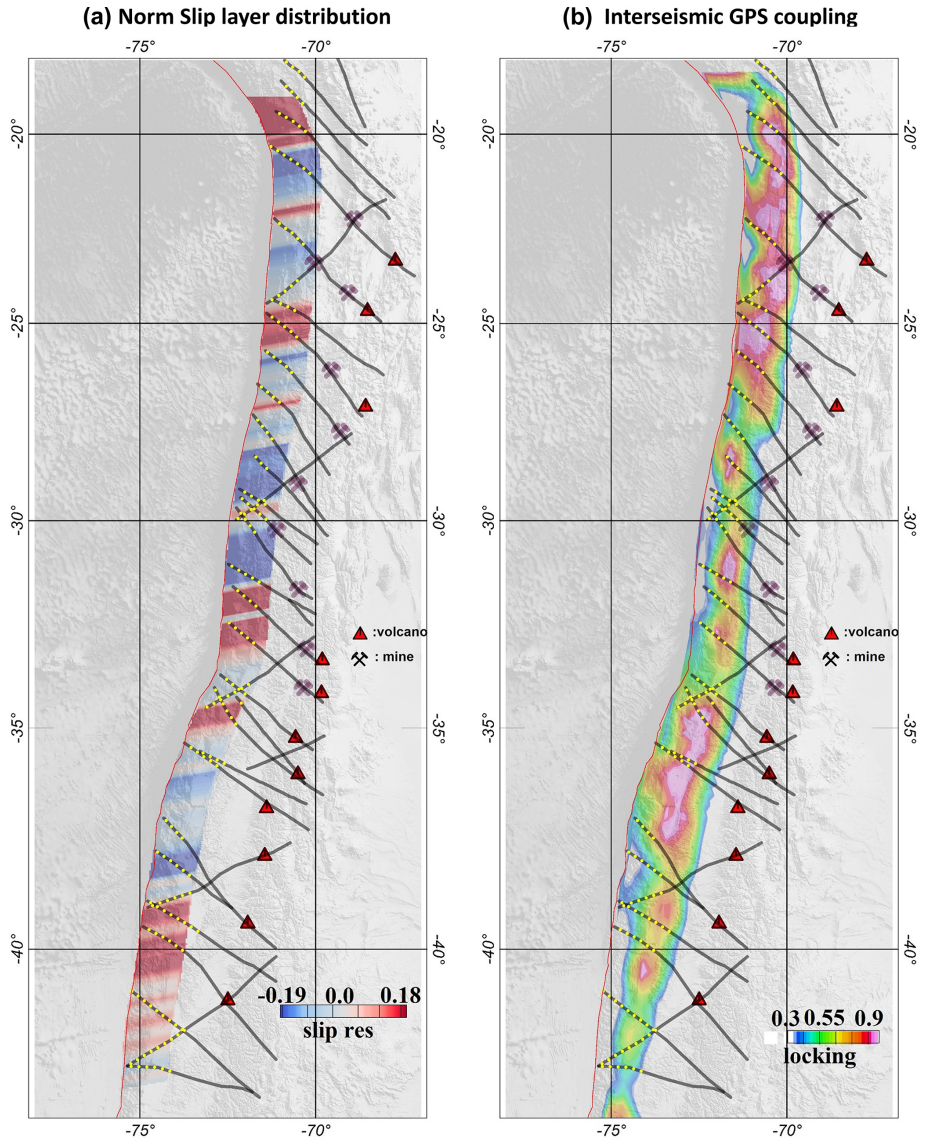

Figure 4. Panel **(a)** shows the normalised residual slip layer viscosity (RSLV: VIS) derived from 1D modelling along profiles separated every 10 km and oriented along the Nazca–South American plate convergence (10° N); as this model involves all of the slip layer, its spatial distribution is represented from the trench until 150 km landward. High relative coupling is associated with high residual slip viscosity (see details of this computation in Sect. S1). Panel **(b)** shows the GPS inter-seismic plate coupling with model 2017 (Burgmann et al., 2005; Chlieh et al., 2008; Loveless and Meade, 2011; McCaffrey et al., 2002; Metois et al., 2012, 2016; Moreno et al., 2010, 2012; Wallace et al., 2004). Locking is restricted to the range between 0.3 to 0.9 in order to enhance the relative coupling along the plate-coupling zone.

$$r_{xy} = \frac{\sum_{i=1}^{n}(x_i - \overline{x})(y_i - \overline{y})}{\sqrt{\sum_{i=1}^{n}(x_i - \overline{x})^2 \sum_{i=1}^{n}(y_i - \overline{y})^2}}, \quad (1)$$

where $\overline{x}$ and $\overline{y}$ are the average value of each variable. This function r_{xy} has values between -1 (opposite correlation) to 1 (direct correlation). Values near zero mean weak or null correlation. In the application of the Pearson correlation in this case, the spatial distribution of TLFs is always the x_i, and the six proxies used in this case are the y_i in each case.

A key property of the Pearson correlation coefficient is its invariance to spatial distribution of samples and scale of the two variables. This property is particularly useful in this case, where we are trying to correlate very different proxies in terms of spatial distribution and scale. The correlation is performed in moving windows bins of 32 km × 32 km, with an overlap of 50 % between correlation estimates. The correlation is calculated in a domain of 140 km width from the trench to the east in the plate-coupling zone, where short-term and long-term processes take place.

TLFs are defined as line traces, but in order to spatially correlate them with the other variables, we add a width, considering potential spatial uncertainties and zones of influence. Thus, the width of each TLF is treated as a Gaussian with a value of 1 in the centre and 0 at the edge, located at 10 km from the centre, representing the deformation zone and the lateral surface covered by the potential fluid release. Such a width of 20 km seems a reasonable number for a fault system of more than 100 km length (> 20 %). In fact, in recorded earthquakes, like the Landers earthquake in 1992 (M_w 7.3), where a rupture length of 85 km has been determined, the shear deformation zone reached 12–16 km (Perrin et al., 2021). Outside the TLF domains, a value of −1 indicates no spatial distribution of TLFs, but in practice this is not relevant because the correlation is focussed inside the TLF domain only. The other six proxies are treated in a different manner, depending on their nature. GPS plate coupling is a spatial variable covering the whole spatial range of the coupling. Looking at the GPS coupling described in Fig. 4b, we can see that most of the plate contact is highly coupled, well above 0.6 almost everywhere; thus, in order to identify some differences in the coupling, we set up the mean value at 0.8. Slip viscosity layer and distance from the shelf brake to the trench are single values varying with latitude that are extended to spatial variables projecting the value landward and following the convergence direction (∼ 10° E). In the case of the slip coupling, a mean value is already removed; thus a mean value of zero is considered. For the shelf brake–trench distance, we use the average separation of 100 km as the mean value. Seismic cumulative density and slip distribution of megathrust events define restrictive domains along the plate-coupling region. These areas are normalised between 1 and 0, and outside the region, a value of −1 is assigned (no data). The same procedure is used for the boundary between historic seismicity segmentation, with a value of 1 in the transition and −1 outside. Since the analysis is restricted to the correlation between TLFs and the six proxies, the correlation only concerns the inner part of the TLFs. Given the nature of each proxy, a low coupling at a given TLF implies a negative Pearson correlation at GPS and viscous coupling, distance from the shelf brake to the trench, and a slip distribution for megathrust events (maximum slip should lie outside the TLF domain). On the contrary, a positive Pearson correlation is expected with the historic segmentation and cumulative seismicity to reflect low coupling at the TLF domain.

The results for each Pearson correlation coefficient spatial distribution are presented in Fig. 5 in a plan view. In Fig. 8, we present the result for the 32 relevant TLFs in terms of the histogram obtained for the Pearson correlation inside the corresponding TLF domain. Over the histogram observations we include an interpretation on the correspondence with a low plate-coupling condition, depending on the shape of the histogram, positive (Pearson correlation biased to the left in GPS, VISC, DIST, and SLIP histograms and biased to the right in the CUMM and HIS histograms), unclear (flat for all the proxies), and negative (Pearson correlation biased to the right in GPS, VISC, DIST, and SLIP histograms and biased to the left in the CUMM and HIS histograms) correlation. Based on this analysis, we qualify the potential of each TLF in terms of its barrier potential (high, ambiguous, and poor). The criteria to establish this qualification consider the following: (a) high potential – at most one correlation is negative, and the majority have a positive correlation; (b) ambiguous – at most two correlations are negative, and at least one correlation is positive; (c) poor – when more than three correlations are negative or none of them is positive.

Some relevant conclusions arise from the spatial analysis of Figs. 5–7 and the histograms in Fig. 8.

1. From the 32 relevant TLFs in terms of plate coupling, 63 % (20 of 32) show a high potential for a barrier behaviour, 31 % (10 of 32) present some ambiguity, and only 6 % of TLFs (2 of 32) show a poor chance to become a barrier domain.

2. For the case of ambiguous potential, almost all of them present at least two positive correlation proxies.

3. For individual histograms, 54 % of histograms show a positive correlation, 28 % are considered ambiguous, and 18 % present a negative correlation.

4. Five out of seven seismotectonic boundary segments present a strong correlation with TLF spatial distribution (Fig. 5). In terms of the particular histogram distribution, 11 out of 13 show a positive correlation, and none of them shows a negative correlation.

5. The cumulative interseismic seismicity (Fig. 5), perhaps the weakest proxy due to the lack of seismic completeness due to the very restricted time window of observation, still shows an almost 100 % direct correlation with the TLF traces where inter-seismic activity developed (TLFs 14–15–16, TLFs 18–20, and TLF 22). In terms of the histogram distribution, it shows a rather similar pattern, with some clear positive correlations in 6 out 18 TLFs and no conclusive solutions in 12 out 18 cases.

6. The spatial distribution of the slip zones of the main megathrust events recorded in the last 50 years show a minimum positive correlation with the spatial distribution of TLFs. As we can see in Fig. 6, less than 20 % of the total slip domains, potential zones of asperities, correlate positively with TLFs. The most conspicuous case against the rule is the slip zone of the Antofagasta 1995 that cut two TLFs (no.7 is Agua Verde–Exploradora and no. 8 is Antofagasta–Chonchi) and, partially, the Tocopilla 2007 event (Mejillones–Llullaillaco TLF 6). Two complementary explanations are proposed in this case: (1) both are small events (8 M_w) compared to the other megathrust events, and (2) not necessarily all TLFs behave as barriers all the time. For the case of the

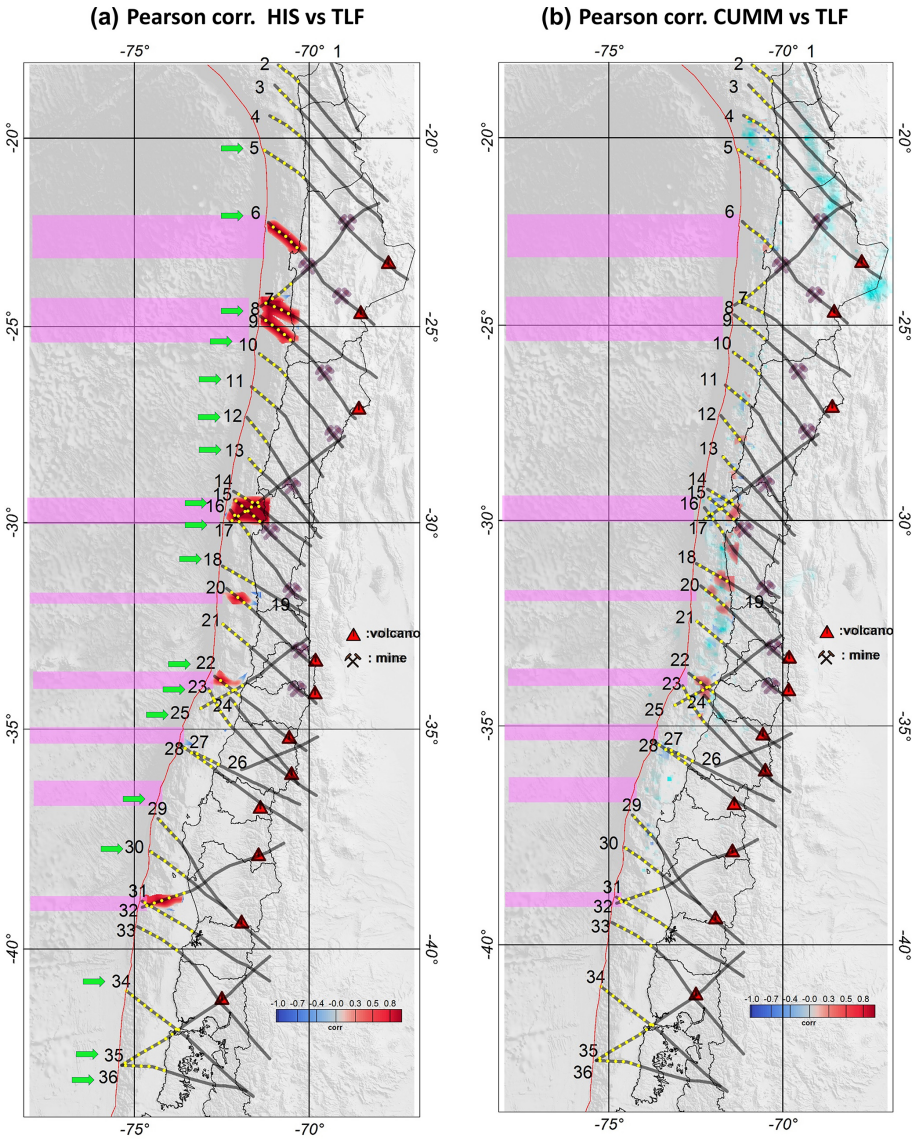

Figure 5. Pearson correlation coefficient between TLFs and **(a)** tectonic segmentation (from Fig. 2a) and **(b)** cumulative seismicity (from Fig. 3a). Colour code ranges from −1 (opposite correlation; blue colours) to 1 (direct correlation; red colours). In panel **(a)**, the green arrow shows the TLFs with high potential as a barrier, according with the criteria established from histograms distribution of Fig. 6. Correlation is only determined in the vicinity of TLFs.

Iquique 2014 event, the seaward extension of Iquique TLF is not well constrained and most likely runs straight from the landward segment, leaving the slip zone entirely to the south of TLF 4. The remaining 80 % lies outside the zone of influence of TLFs. In the histogram distribution, the same pattern is observed, with 57 % having a negative Pearson correlation (or positive correlation in terms of low plate coupling), 26 % having an ambiguous solution, and 17 % having a positive Pearson correlation. It is important to note that in several histograms of this proxy, a positive correlation is adopted when a low flat response is observed, but on the left-hand side there is a single column saturated at the maximum value for correlation −1 (most of the TLFs are empty or, in other words, the slip zone lies outside the TLF domain).

7. In the GPS plate coupling, for the TLF Pearson correlation coefficient (Fig. 6), 50 % of the cases show a negative correlation (low relative coupling), whereas 30 % show some mix results, with the negative correlation concentrated in the deeper parts of the coupling, and only in 20 % of the cases does a positive correlation hold, mostly concentrated in the coupling zone of the Antofagasta 1995 and Tocopilla 2007 earth-

quakes, and probably linked with some post-seismic effects. Consistently, in 18 out of 32 (56 %) histogram responses (Fig. 8), the low coupling correlation is observed, whereas in 10 out of 32 (31 %), the response is ambiguous, and the remaining 13 % are associated with relatively high GPS coupling. We acknowledge that these values are very much conditioned by the choice of the threshold of 80 % to separate high to low GPS coupling, but the aim is to identify less coupled domains in a signal almost saturated with high values.

8. The same type of analysis was performed for the slip layer viscosity TLF Pearson correlation coefficient (Fig. 7). In 50 % of the case, the correlation is opposite (low-viscosity slip zones correspond with the location of TLFs). In 15 % of the cases, we observed mixed results, whereas in 35 % of the cases, the correspondence is positive. Similar results are obtained with histogram responses (Fig. 8); in 17 out of 32 (53 %), the low coupling correlation is observed, whereas in 6 out of 32 (19 %) the response is ambiguous, and the remaining 28 % is associated with relative high slip viscosity. One important limitation of this approach is the 1D approximation of an inherently 3D process. This fact is probably the main reason for its relatively low positive response compared to the other proxies. Finally, Fig. 5c shows the Pearson correlation coefficient for the distance from the shelf brake to the trench. In this case, the closest shelf brake to the trench at TLF intersection is a 36 %; the same number of cases show an opposite behaviour, and only 28 % present mixed results. In terms of the histogram distribution (Fig. 8), the same tendency is observed but with a higher predominance of a shorter distance shelf brake–trench (44 %), whereas the opposite is observed in 34 % of the cases, and 22 % show an ambiguous response. This is the proxy that shows the lowest level of positivity, probably due to the fact that other processes are also involved in the uplift of the peninsula regions, for instance, the density of the crust and its relative buoyancy.

As we point out earlier in the text, none of the proxies by themselves has the merit to account for the degree of coupling along the subduction zone, and the results emanating from the Pearson correlation demonstrate that. However, when we integrated the individual results, 63 % of the TLFs can potentially behave as barrier, and only in two cases (6 %) are chances poor. In the remaining 31 % of the cases, represented as ambiguous cases, there is still some evidence of positive correlations in more than one proxy. In Fig. 5a, we include a reference for the TLFs showing high potential to become a barrier (green arrow), and we can see that in almost all the cases they are consistent with the tectonic segmentation derived from the historic seismicity. One peculiar distribution of potentially active barrier domains is observed between 25–30° S, the zone with less historical seismicity (Fig. 2). On the other hand, not necessarily all the TLFs behave as barriers, due to lack of favourable orientation, depth extent, age, dip angle, and fluid content, among other uncertainties. Therefore, we consider that the previous semiquantitative analysis including all the proxies supports the presence of a geological signal of low plate coupling when a TLF is present. In the next section, we propose a conceptual mechanism to explain this phenomenon.

3.2 A simple conceptual barrier model: misoriented TLFs as a store/release of fluids during the seismic cycle

Comparing the spatial distribution of the seaward extension of the TLFs and the previously discussed first-order conditioning factors of the tectonic segmentation in the Andes (Sect. 2) and the cross-correlation described in Sect. 4.1, we can make the following conclusions.

1. The coastal termination of a TLF generally occurs close to a peninsula, where the shortest trench–coast distance is observed, in spatial correspondence with the zones of negative RSLV (weak viscous coupling) and, in some cases, also corresponding to zones of weak GPS coupling. However, it should be noted that the degrees of coupling inferred via RSLV and GPS do not map similar observation time windows, covering geological (Myr) vs. seismic cycle (300–500 years) time frames, respectively.

2. During the last 60 years, slip displacements during the major megathrust earthquakes in the margin of Chile tend to be bounded by the coastal termination of a TLF in their northern and southern boundaries. Thus, if these slip zones represent a spatial distribution of asperities, the TLFs correspond to zones potentially associated with barriers, consistent with the long-term low coupling inferred from RSLV, GPS plate coupling, and the distributions of peninsulas in the previous long-term observations.

3. Cumulative seismic activity in the last 20 years tends to nucleate in the vicinity of the seaward termination of the TLFs, normally with the development of seismic swarms of 100–300 events of medium to low magnitudes during periods of several weeks at most.

4. The geological record demonstrates that TLFs are long-lived structures of high permeability in comparison with the surrounding crust, and most likely the underlying mantle as well, and are thus potentially efficient fluid storage structures.

The previous observations provide the grounds to propose a simple conceptual model to understand the role played by TLFs in the tectonic segmentation of a convergent margin.

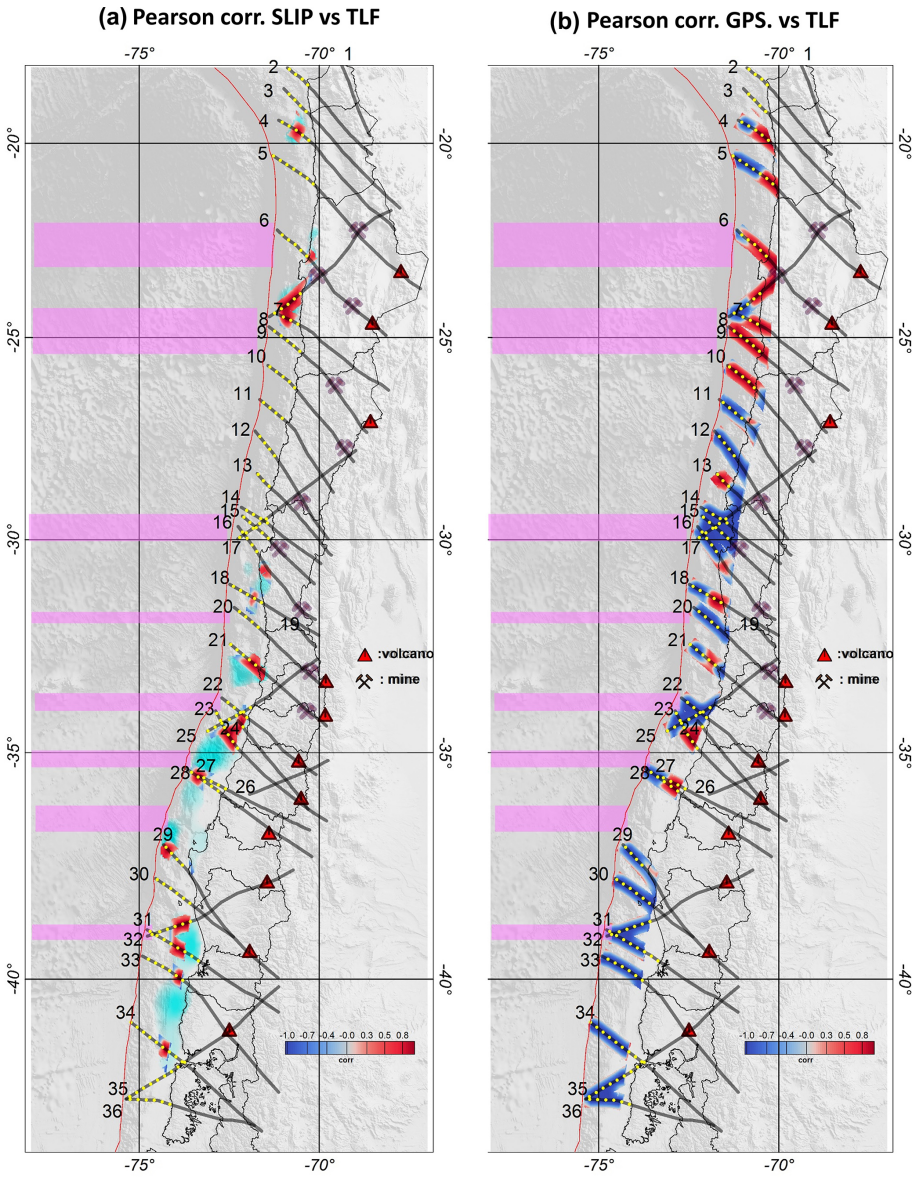

Figure 6. Pearson correlation coefficient between TLFs and **(a)** normalised seismic slip (from Fig. 2b) and **(b)** GPS coupling (from Fig. 4b). Colour code ranges from −1 (opposite correlation; blue colours) to 1 (direct correlation; red colour). Correlation is only determined in the vicinity of TLFs.

These observations consistently show that TLFs in the seismogenic zone are spatially correlated with long-term and short-term evidence of weak coupling behaviour. The long-term evidence involves geological processes that build up during many seismic cycles, over a time frame of millions of years, including low values of slip layer viscosities and correspondence with the spatial distribution of peninsulas. The short-term evidence involves fragments of the seismic cycle over a time frame shorter than 500 years that are characterised by weak coupling zones as inferred by inter-seismic GPS observations, the flanks of slip zones of recent megathrust events, and the boundaries that delimit the historical record of major events. Overall, these observations consistently show that TLF domains are likely candidates for barrier zones.

From basic principles, the strength of a fault is controlled by the friction at the discontinuity plane. According to Amonton's law, the fault strength is proportional to the product of the normal stress and the static or dynamic friction (e.g. Scholz, 1990). In the presence of fluids, pore pressure reduces the normal stress, thereby reducing the strength of the fault (e.g. Scholz, 1990), eventually to zero, if the pore pressure reaches the lithostatic pore pressure. Under these supra-lithostatic fluid pressure conditions, even faults

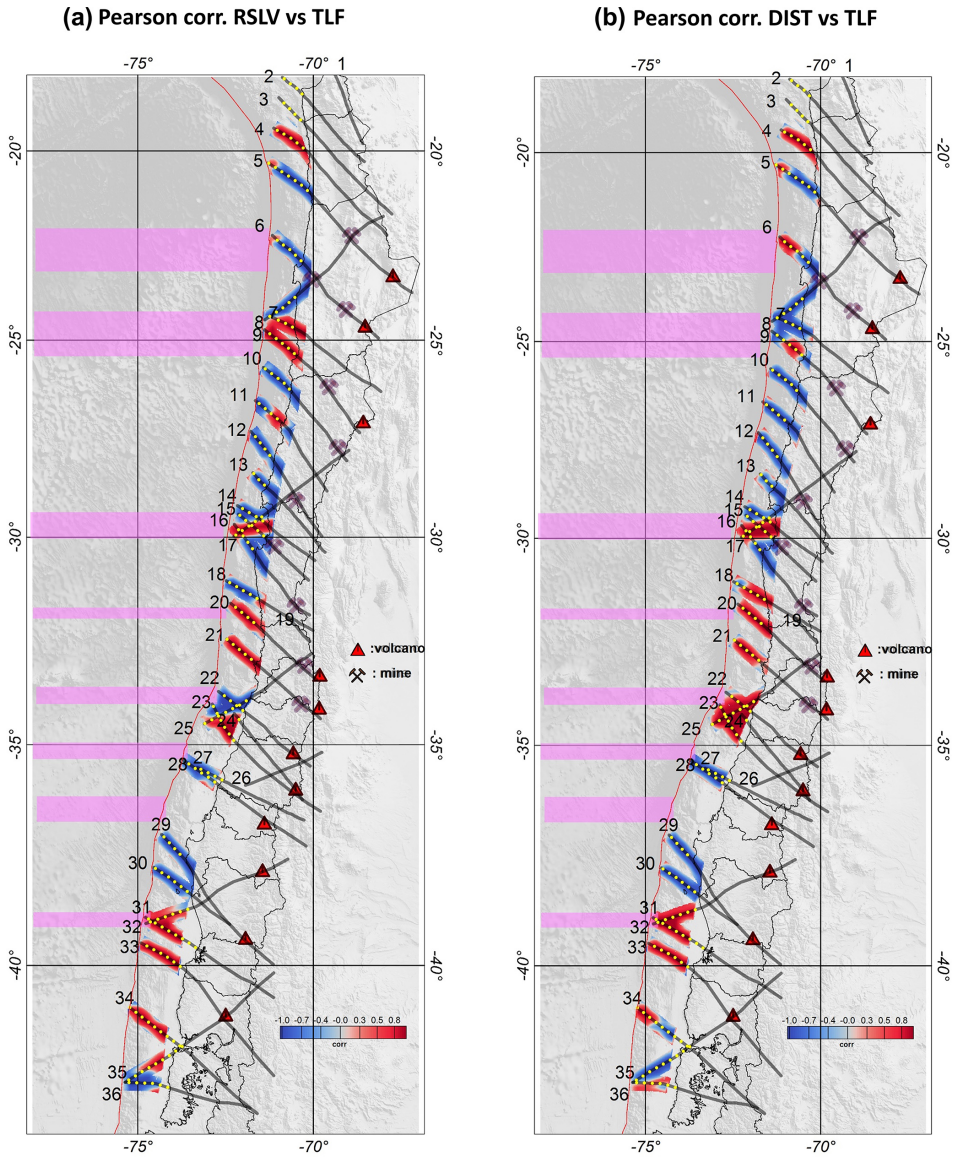

Figure 7. Pearson correlation coefficient between TLFs and tectonic slip viscosity (from Fig. 4a) **(a)** and distance from the trench to the shelf brake (from Fig. 3b) **(b)**. Colour code ranges from −1 (opposite correlation; blue colour) to 1 (direct correlation; red colour). Correlation is only determined in the vicinity of TLFs.

that are strongly misoriented for frictional reactivation under the prevailing stress field can be reactivated, focusing the discharge of large amounts of overpressured fluids and acting as a fault–valve (Sibson, 1990; Cox, 2016). Indeed, Cox (2016), showed that, under supra-lithostatic fluid pressure conditions, the typical seismic response in the fault corresponds to microseismic swarms, which, according to Sibson (2020), would concentrate at the roots of the fault system. In the case of a TLF, which is a long-lived structure transecting the whole lithosphere (e.g. Lutz et al., 2022), the root of the fault system at the Andean convergent margin corresponds to the subduction channel. Low fault strength at subduction zones can be equated to barrier zones where convergence is mostly accommodated by creep and/or micro-seismicity. The hydration of the subducting slab during its bending in the outer rise region has been widely documented in different subduction margins (e.g. Shillington et al., 2015; Contreras-Reyes et al., 2007; Moscoso and Grevemeyer, 2015; Ranero and Sallarès, 2004; Fujie et al., 2018, among others), as has the slab's subsequent dehydration during subduction (Barriga et al., 1992; Maekawa et al., 1993; Peacock, 1993). Mantle hydrous phases (serpentinites) have also been observed in forearc regions at subduction margins (e.g. Hyndman and Peacock, 2003; Xia et al., 2015; Hansen et al., 2016), further demonstrating that subduction systems transport large amounts of water; however, the amount of water

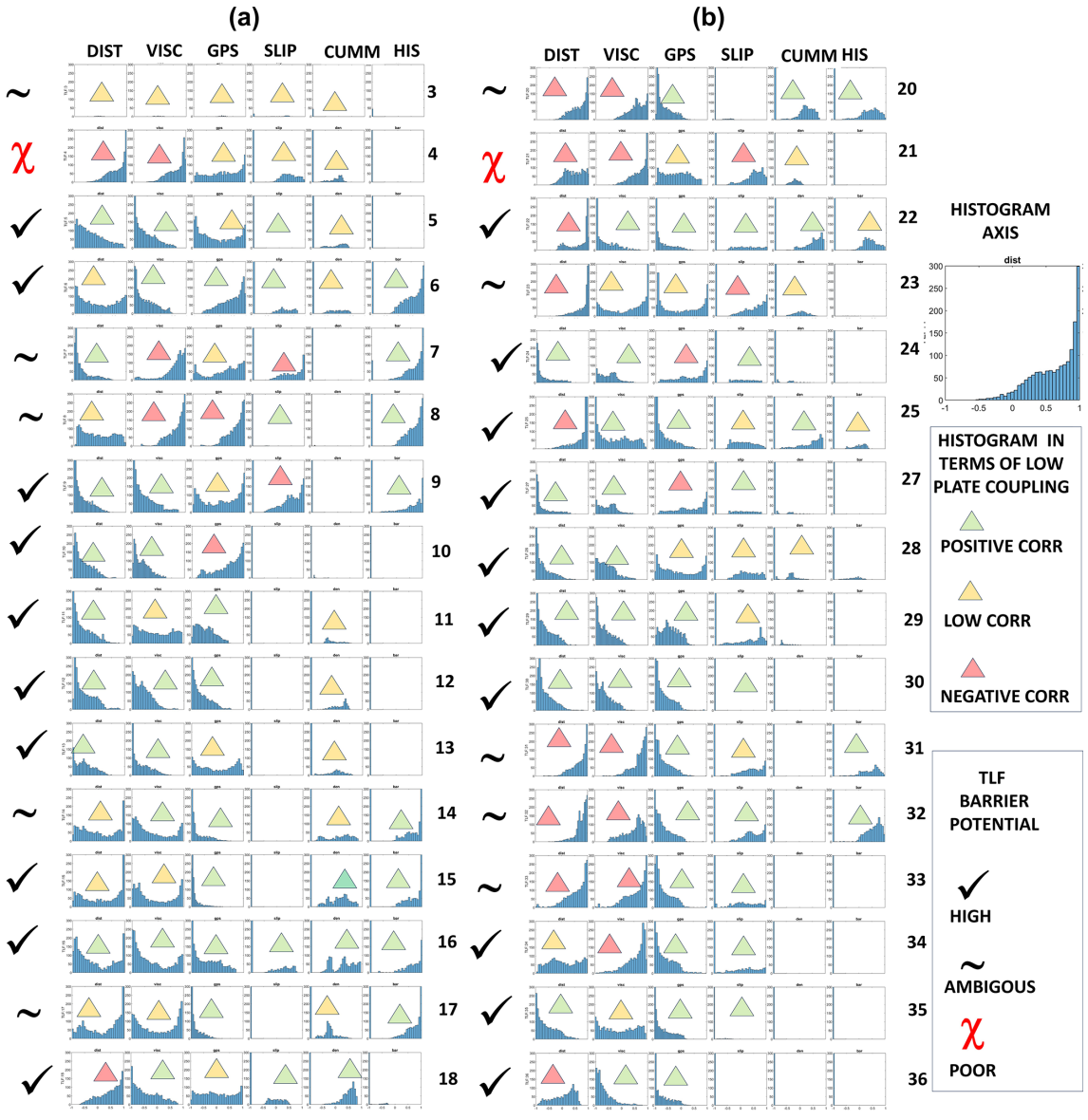

Figure 8. Histogram diagrams for the Pearson correlation in each TLF (six histograms for each TLF). Histogram interpretation and TLF qualification as a potential barrier is indicated in inlet. TLF number is indicated on the left of each panel (a higher-resolution version of this image is provided in the Supplement). Correlation type is indicated by triangles in each histogram, while the estimate TLF barrier potential (high to poor) is indicated by symbols on the left side of each histogram.

transported is still unknown (Miller et al., 2021). On the other hand, fluid flow in porous media is governed by Darcy's law, which is in the opposite direction to the hydraulic head and proportional to the hydraulic permeability. Numerical models (Menant et al., 2020) have been used to determine the path of overpressured fluid flow along the subduction channel and how strong/weak frictional channels condition the flow (weak frictional channel zones percolate more water upwards compared to strong frictional channel zones). These two domains determine the location of weak and strong coupling zones at the plate contact. Thus, according to basic principles and numerical models, water concentrates in zones of high permeability.

The geological record on land shows that, in the Andean margin, TLFs are associated with ore deposits clustered at the intersection of magmatic arcs that become progressively younger eastward (Piquer et al., 2016, 2021a; Yáñez and Rivera, 2019; Farrar et al., 2023; Wiemer et al., 2023), covering the full tectonomagmatic history during the Mesozoic and Cenozoic. Local seismic networks deployed in northern and central Chile also show alignments of seismic activity along some TLF systems (Yánez and Rivera, 2019; Piquer et al., 2019, 2021a; Sielfeld et al., 2019; Pearce et al.,

2020). These long- and short-term observations indicate the presence of long-lived high-permeability domains along the TLF systems in the Andean margin of northern and central Chile. Therefore, we postulate that TLFs act as fluid sinks in the forearc region, following a continental-scale fault–valve behaviour, carrying the fluids released by slab dehydration and transported from distal locations through the subduction channel and discharging the fluids upwards and laterally through the TLFs. Thus, if the proposed mechanism operates for long periods of time, the fluid distribution at the plate contact should show an uneven distribution of fluid, delimitating domains of weak and strong friction channels, which would act as seismic barriers and asperities, respectively. In this context, the spatial distribution of TLFs would be associated with barriers that delimitate the tectonic segmentation. In the proposed model, tremor or swarm seismic activity represent episodic fluid release from TLFs that are poorly oriented with respect to the regional tectonic stress – in this case, the NW-striking fault systems are oriented at a high angle relative to the ENE convergence direction. This model provides a causal link between the presence of TLFs in the upper plate and the distribution of barrier and asperity domains in the plate interface. A schematic cartoon of this model is presented in Fig. 9.

Our proposed conceptual model in which TLFs promote the development of barrier domains along the subducting margin through the enhancement of fluid pressure complement other processes at subduction zones that also enhance the budget of localised fluids at the plate contact, including among them the collision of aseismic ridges and fracture zones and the bending of the subducting plate (e.g. Ranero et al., 2008, 2005; Martinez-Loriente et al., 2019; Arai et al., 2024). In the Nazca–South America plate interaction, authors had highlighted this increase in fluids at passive ridges such as the Taltal ridge, 33° S (Leon-Rios et al., 2024); the Juan Fernández Ridge, 33.5° S (Garrido et al., 2002); and fracture zones such as the Challenger Fracture Zone, 30° S (Poli et al., 2017; Maksymowicz, 2015). The volume of fluids in aseismic ridges is enhanced by oceanic water percolation along the thicker oceanic crust, while in fracture zones it is as a result of the high permeability that provides a mechanism to increase water storage prior to the subduction. These complementary mechanisms share a common origin at the subducting plate, and in the particular case of the Nazca Plate, they are oblique to the margin (roughly NE). Thus, the main difference with the proposed model is their along-strike migration with time, while in the proposed mechanism, TLFs belong to the overriding plate.

3.3 Implications

If TLFs act as low-friction domains (barriers) due to their capacity to store fluids released from the subducting slab and thereby dry out neighbouring zones of the subduction channel to promote the development of a high-friction domain (asperity), we can envision a series of implications derived from the proposed model.

The most relevant implication is the geological control of barrier zones. This geological control exerted by high-permeability domains in the continental lithosphere (TLFs) implies a spatial control of barrier zones, and thus the seismotectonic segmentation should be stable for several seismic cycles, as long as the capacity of TLFs to store fluids is maintained. If this scenario is correct, the estimate of the seismic risk associated with each seismotectonic segment can be assessed based on empirical fault length laws (e.g. Anderson et al., 2017). In this context, interplate seismic swarms and slow seismic events that develop in the vicinity of TLF zones would be a mechanism for the steady release of seismic energy.

As discussed previously, several TLFs have been identified in the Andean margin; however, little is known about their origin, width, dip, depth, extent, and capacity to behave as a water sink. Therefore, further study is needed to postulate a reliable map of barrier domains in this subduction system.

On the other hand, seismic barriers/asperities would be conditioned by the capacity of barrier zones to mobilise and store fluids and would thus be relatively stable in space but with a variable behaviour during several seismic cycles. If the age of the subducted slab conditions the water budget at the plate interface (Ruepke et al., 2004), the progressive age increase from south to north in this margin (from 0 to 45 Ma) would be a controlling factor for the efficiency of the TLF barrier hypothesis. Although this implication is highly speculative, the historical record shows that the largest megathrust events at the margin have occurred in southern Chile, including the 9.3 M_w 1960 Valdivia earthquake, the largest event recorded worldwide.

4 Conclusions

Based on first-order geological and geophysical observations of the Nazca–South America plate convergence, we propose a conceptual model to understand the tectonic segmentation in the Andean region.

Observations include historical seismicity and the associated seismotectonic segmentation. Major thrust events occurred in the region in the last 60 years, defining domains of asperities. GPS and viscous plate coupling that provide independent proxies to establish the potential domains of barriers (low plate coupling) and asperities (high plate coupling). Location of low-plate-coupling domains is further associated with the spatial distribution of peninsulas (less basal erosion) and cumulative seismicity during the inter-seismic period (slow interplate seismic events and creeping, which are associated with fluid release).

A key element in the model is played by trans-lithospheric faults (TLFs). Landward, this TLF system concentrates the occurrence of major hydrothermal ore deposits and some

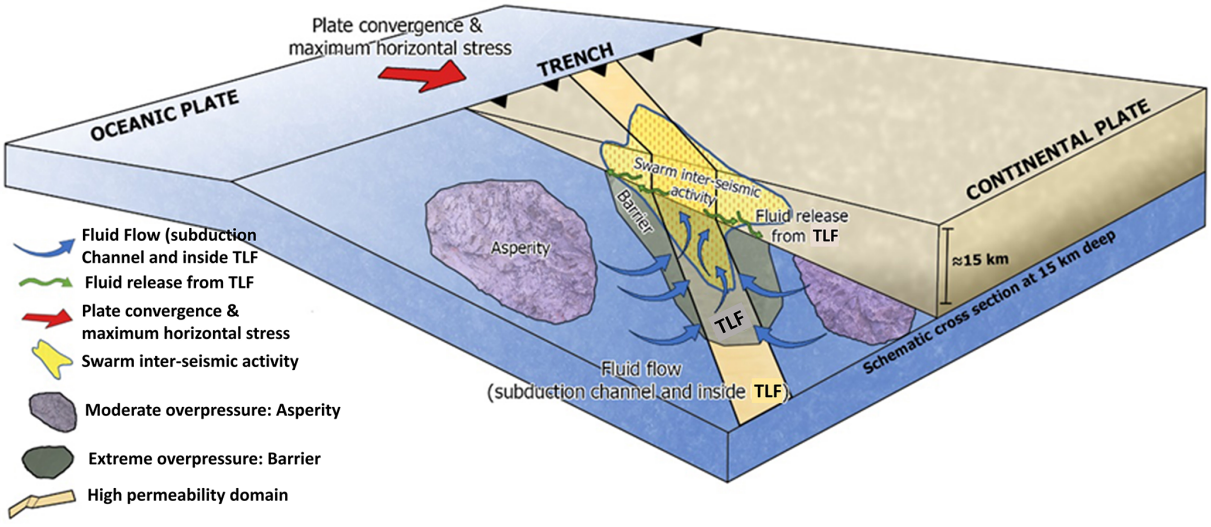

Figure 9. Schematic conceptual model of fluid transport towards TLFs, following different paths in the subduction channel, as well as moving upwards within the TLFs. This model proposes that TLFs are sink domains of slab-derived fluids that promote the development of barrier zones and dry out the neighbouring domains where asperities develop. Swarm clustering in spatial association with the TLFs represents a mechanism for the quasi-creep release of energy within the barrier zone.

active volcanism, denoting their intrinsic high permeability. Thus, at their seaward edge, the TLF domains act as sink and release of fluids during the seismic cycle. The fluid is captured from the slab through the subducting channel and continuously releases to the plate contact, promoting the growth of barriers beneath them (excess of fluids) and asperities laterally (reduction in fluid content).

If the interaction of first-order continental structures and the fluid content of the subducting slab plays a central role in the seismotectonic segmentation of convergence zones, a carefully understanding of the overriding plate geology and associated structures could be instrumental to better understand the associated seismic risk.

Data availability. The topographic/bathymetric data extracted from a public source, ETOPO 2022, at https://doi.org/10.25921/fd45-gt74 (NOAA National Centers for Environmental Information, 2022).

Supplement. The supplement related to this article is available online at: https://doi.org/10.5194/se-15-1319-2024-supplement.

Author contributions. GYC: conceptualization, methodology, software, writing original draft preparation, and investigation. JPR: conceptualization, methodology, investigation, reviewing, and text/figure editing. ORH: conceptualization, methodology, investigation, reviewing, and text/figure editing.

Competing interests. The contact author has declared that none of the authors has any competing interests.

Disclaimer. Publisher's note: Copernicus Publications remains neutral with regard to jurisdictional claims made in the text, published maps, institutional affiliations, or any other geographical representation in this paper. While Copernicus Publications makes every effort to include appropriate place names, the final responsibility lies with the authors.

Acknowledgement. This research was partially supported by a Fondef project (grant no. D10I1027). Jose Piquer R. acknowledges support from ANID-FONDECYT (grant no. 11181048) and the Amira Global P1249 project. The authors would also like to thank Guillermo Booth-Rea and one anonymous reviewer for their valuable observations, as the paper has been greatly improved with the observations made by both reviewers.

Financial support. This research has been supported by the Fondo de Fomento al Desarrollo Científico y Tecnológico (grant no. D10I1027) and the Fondo Nacional de Desarrollo Científico y Tecnológico (grant no. 11181048).

Review statement. This paper was edited by Simone Pilia and reviewed by Guillermo Booth-Rea and one anonymous referee.

References

Aki, K.: Asperities, barriers, characteristic earthquakes and strong motion prediction, J. Geophys. Res., 5867–5872, 89, https://doi.org/10.1029/JB089iB07p05867, 1984.

Anderson, J. G., Biasi, G. P., and Wesnousky, S.: Fault-scaling relationships depend on the average fault-slip rate, B. Seismol. Soc. Am., 107, 2561–2577, https://doi.org/10.1785/0120160361, 2017.

Angermann, D., Klotz, J., and Reigber, C.: Space-geodetic estimation of the Nazca–South America Euler vector, Earth Planet. Sc. Lett., 171, 329–334, https://doi.org/10.1016/S0012-821X(99)00173-9, 1999.

Arai, R., Shiraishi, K., and Nakamura, Y., Fujie, G., Miura, S., Kodaira, S., Bassett, D., Takahashi, T., Kaiho, Y., Hamada, Y., Mochizuki, K., Nakata, R., Kinoshita, M., Hashimoto, Y., and Okino, K.: Thick slab crust with rough basement weakens interplate coupling in the western Nankai Trough, Earth Planets Space, 76, 73, https://doi.org/10.1186/s40623-024-02025-4, 2024.

Aron, F., Allmendinger, R., Cembrano, J., González, G., and Yáñez, G.: Permanent Forearc Extension and Seismic Segmentation: Insights from the 2010 Maule Earthquake, Chile, J. Geophys. Res.-Sol. Ea., 118, 724–739, https://doi.org/10.1029/2012JB009339, 2013.

Arriagada, C., Roperch, P., Mpodozis, C., Dupont-Nivet, G., Cobbold, P. R., Chauvin, A., and Cortés, J.: Paleogene clockwise tectonic rotations in the forearc of central Andes, Antofagasta region, northern Chile, J. Geophys. Res.-Sol. Ea., 108, 2032, https://doi.org/10.1029/2001JB001598, 2003.

Avouac, J. P.: Dynamic Processes in Extensional and Compressional Setings – Mountain Building: From Earthquakes to Geological Deformation, Treatise on Geophysics, 6, 377–439, 2007.

Barrientos, S. E. and Ward, S. N.: The 1960 Chile earthquake: inversion for slip distribution from surface deformation, Geophys. J. Int., 103, 589–598, https://doi.org/10.1111/j.1365-246X.1990.tb05673.x, 1990.

Barriga, F. J. A. S., Fyfe, W. S., Landefeld, L. A., and Ribeiro, A.: Mantle eduction: Tectonic fluidisation at depth, Earth-Sci. Rev., 32, 123–129, 1992.

Bilek, S. L., Schwartz, S. Y., and DeShon, H. R.: Control of seafloor roughness on earthquake rupture behavior, Geology, 31, 455–458, 2003.

Brace, W. F. and Byerlee, J. D.: Stick-Slip as a Mechanism for Earthquakes, Science, 153, 990–992, https://doi.org/10.1126/science.153.3739.990, 1966.

Bürgmann, R., Kogan, M. G., Steblov, G. M., Hilley, G., Levin, V. E., and Apel, E.: Interseismic coupling and asperity distribution along the Kamchatka subduction zone, J. Geophys. Res., 110, B07405, https://doi.org/10.1029/2005JB003648, 2005.

Burridge, R. and Knopoff, L.: Model and theoretical seismicity, B. Seismol. Soc. Am., 57, 341–371, https://doi.org/10.1785/BSSA0570030341, 1967.

Cahill, T. and Isacks, B. L.: Seismicity and shape of the subducted Nazca Plate, J. Geophys. Res., 97, 17503–17529, 1992.

Calle-Gardella, D., Comte, D., Farías, M., Roecker, S., and Rietbrock, A.: Three-dimensional local earthquake tomography of pre-Cenozoic structures in the coastal margin of central Chile: Pichilemu fault system, J. Seismol., 25, 521–533 https://doi.org/10.1007/s10950-021-09989-w, 2021.

Cembrano, J. and Lara, L.: The link between volcanism and tectonics in the southern volcanic zone of the Chilean Andes: A review, Tectonophysics, 471, 96–113, 2009.

Chernicoff, C. J., Richards, J. P., and Zappettini, E. O.: Crustal lineament control on magmatism and mineralization in northwestern Argentina: geological, geophysical, and remote sensing evidence, Ore Geol. Rev., 21, 127–155, 2002.

Chlieh, M., De Chabalier, J. B., Ruegg, J. C., Armijo, R., Dmowska, R., Campos, J., and Feigl, K. L.: Crustal deformation and fault slip during the seismic cycle in the North Chile subduction zone, from GPS and InSAR observations, Geophys. J. Int., 158, 695–711, 2004.

Chlieh, M., Avouac, J. P., Sieh, K., Natawidjaja, D. H., and Galetzka, J.: Heterogeneous coupling of the Sumatran megathrust constrained by geodetic and paleogeodetic measurements, J. Geophys. Res., 113, B05305, https://doi.org/10.1029/2007JB004981, 2008.

Comte, D., Eisenberg, A., Lorca, E., Pardo, M., Ponce, L., Saragoni, R., Singh, S. K., and Suárez, G.: The 1985 Central Chile Earthquake: A Repeat of Previous Great Earthquakes in the Region?, Science, 233, 449–453, 1986.

Contreras-Reyes, E., Grevemeyer, I., Flueh, E. R., Scherwath, M., and Heesemann, M.: Alteration of the subducting oceanic lithosphere at the southern central Chile trench–outer rise, Geochem. Geophy. Geosy., 8, Q07003, https://doi.org/10.1029/2007GC001632, 2007.

Cox, S. F.: Injection-driven swarm seismicity and permeability enhancement: implications for the dynamics of hydrothermal ore systems in high fluid-flux, overpressured faulting regimes, Econ. Geol., 111, 559–587, 2016.

Creixell, C., Parada, M. A., Morata, D., Vásquez, P., Pérez de Arce, C., and Arriagada, C.: Middle-Late Jurassic to Early Cretaceous transtension and transpression during arc building in Central Chile: evidence from mafic dike swarms, Andean Geol., 38, 37–63, 2011.

Delouis, B., Monfret, T., Dorbath, L., Pardo, M., Rivera, L., Comte, D., Haessler, H., Caminade, J. P., Ponce, L., Kausel, E., and Cisternas, A.: The $M_w = 8.0$ Antofagasta (northern Chile) earthquake of 30 July 1995: A precursor to the end of the large 1877 gap, B. Seismol. Soc. Am., 87, 427–445, https://doi.org/10.1785/BSSA0870020427, 1997.

Delouis, B., Nocquet, J. M., and Vallée, M.: Slip distribution of the February 27, 2010 $M_w = 8.8$ Maule Earthquake, central Chile, from static and high-rate GPS, InSAR, and broadband teleseismic data, Geophys. Res. Lett., 37, L17305, https://doi.org/10.1029/2010GL043899, 2010.

Espinoza, M., Montecino, D., Oliveros, V., Astudillo, N., Vásquez, P., Reyes, R., Celis, C., González, R., Contreras, J., Creixell, C., and Martínez, A.: The synrift phase of the early Domeyko Basin (Triassic, northern Chile): Sedimentary, volcanic, and tectonic interplay in the evolution of an ancient subduction-related rift basin, Basin Res., 31, 4–32, 2019.

Farías, M., Comte, D., Roecker, S., Carrizo, D., and Pardo, M.: Crustal extensional faulting triggered by the 2010 Chilean Earthquake: The Pichilemu Seismic Sequence, Tectonics, 30, TC6010, https://doi.org/10.1029/2011TC002888, 2011.

Farrar, A. D., Cooke, D. R., Hronsky, J. M. A., Wood, D. G., Benavides, S., Cracknell, M. J., Banyard, J. F., Gigola, S., Ireland, T., Jones, S. M., and Piquer, J.: A Model for the lithospheric

architecture of the Central Andes and the localization of giant porphyry copper deposit clusters, Econ. Geol., 118, 1235–1259, https://doi.org/10.5382/econgeo.5010, 2023.

Fedotov, S. A.: On seismic cycle, possibility of quantitative seismic regionalization and long-term seismic prediction, in: Seismic Zoning of the USSR, edited by: Medvedev, S., Nauka, Moscow, 121–150, 1968.

Fischer, T.: Control estructural sobre la circulación de magmas y fluidos hidrotermales Miocenos y Cuaternarios en el sector de La Invernada, Región del Maule, Chile, Universidad Austral de Chile, Valdivia, 314, 2021.

Forsyth, D., Yang, W. Y., Mangriotis, M. D., and Shen, Y.: Coupled seismic slip on adjacent oceanic transform faults, Geophys. Res. Lett., 30, 20–21, 2003.

Fujie, G., Kodaira, S., Kaiho, Y., Yamamoto, Y., Takahashi, T., Miura, S., and Yamada, T.: Controlling factor of incoming plate hydration at the north-western Pacific margin, Nat. Commun., 9, 3844, 2018.

Gana, P., Wall, R., and Gutiérrez, A.: Mapa Geológico del Área de Valparaíso – Cuaracaví. Regiones de Valparaíso y Metropolitana, Mapas Geológicos No. 1, Escala 1 : 100 000, Servicio Nacional de Geología y Minería, Chile, ISSN 0717-2532, 1996.

Garrido, I., Cembrano, J., Siña, A., Stedman, P., and Yáñez, G.: High magma oxidation state and contractional deformation: key factors in the generation of Andean porphyry copper deposits, Central Chile (31–34° S), Rev. Geol. Chile, 29, 3–14, 2002.

Geersen, J., Ranero, C., and Barckhausen, U.: Subducting seamounts control intraplate coupling and seismic rupture in the 2014 Iquique earthquake area, Nat. Commun., 6, 8267, https://doi.org/10.1038/ncomms9267, 2015.

Giambiagi, L., Álvarez, P., Creixell, C., Mardonez, D., Murillo, I., Velásquez, R., Lossada, A., Suriano, J., Mescua, J., and Barrionuevo, M.: Cenozoic Shift From Compression to Strike-Slip Stress Regime in the High Andes at 30° S, During the Shallowing of the Slab: Implications for the El Indio/Tambo Mineral District, Tectonics, 36, 2714–2735, https://doi.org/10.1002/2017TC004608, 2017.

Glodny, J., Echtler, H., Collao, S., Ardiles, M., Burón, P., and Figueroa, O.: Differential Late Paleozoic active margin evolution in South-Central Chile (37° S–40° S) – The Lanalhue Fault Zone, J. S. Am. Earth Sci., 26, 397–411, https://doi.org/10.1016/j.jsames.2008.06.001, 2008.

González-Vidal, D., Moreno, M., Sippl, C., Baez, J. C., Ortega-Culaciati, F., Lange, D., Tilmann, F., Socquet, A., Bolte, J., Hormazabal, J., Langlais, M., Morales-Yáñez, C., Melnick, D., Benavente, R., Münchmeyer, J., Araya, R., and Heit, B.: Relation between oceanic plate structure, patterns of interplate locking and microseismicity in the 1922 Atacama seismic gap, Geophys. Res. Lett., 50, e2023GL103565, https://doi.org/10.1029/2023GL103565, 2023.

Gutscher, M. A., Malavielle, J., Lallemand, S., and Collot, J. Y.: Tectonic segmentation of the north Andean margin: impact of the Carnagie Ridge collision, Earth Planet. Sc. Lett., 168, 255–270, 1999.

Haberland, C., Rietbrock, A., Lange, D., Bataille, K., and Hofmann, S.: Interaction between forearc and oceanic plate at the south-central Chilean margin as seen in local seismic data, Geophys. Res. Lett., 33, 1–5, 2006.

Hansen, S., Schmandt, B., Levander, A., Kiser, E., Vidale, J. E., Abers, G. A., and Creager, K. C: Seismic evidence for a cold serpentinized mantle wedge beneath Mount St Helens, Nat. Commun., 7, 13242, https://doi.org/10.1038/ncomms13242, 2016.

Hayes, G.: Slab2 – A Comprehensive Subduction Zone Geometry Model: U. S. Geological Survey data release, https://doi.org/10.5066/F7PV6JNV, 2018.

Hayes, G., Herman, M., Barnhart, W., Furlong, K. P., Riquelme, S., Benz, H. M., Bergman, E., Barrientos, S., Earle, P. S., and Samsonov, S.: Continuing megathrust earthquake potential in Chile after the 2014 Iquique earthquake, Nature, 512, 295–298, https://doi.org/10.1038/nature13677, 2014.

Heidarzadeh, M., Murotani, S., Satake, K., Ishibe, T., and Gusman, A. R.: Source model of the 16 September 2015 Illapel, Chile M_{w} 8.4 earthquake based on teleseismic and tsunami data, Geophys. Res. Lett., 43, 643–650, 2016.

Hyndman, R. D. and Peacock, S. M.: Serpentinization of the forearc mantle, Earth Planet. Sc. Lett., 212, 417–432, 2003.

Kay, S. M. and Mpodozis, C.: Magmatism as a probe to the Neogene shallowing of the Nazca plate beneath the modern Chilean flat slab, J. S. Am. Earth Sci., 15, 39–57, 2002.

Kimura, G., Yamaguchi, A., and Masataka, M.: Upper-plate tectonic hysteresis and segmentation of the rupture area during seismogenesis in subduction zones – A case study of the Nankai Trough, in: Geology and Tectonics of Subduction Zones: A Tribute to Gaku Kimura, edited by: Byrne, T., Underwood III, M. B., Fisher, D., McNeill, L., Saffer, D., Ujiie, K., Yamaguchi, A., Geological Society of America, https://doi.org/10.1130/2018.2534(05), 2018.

Kohler, P. A.: Geología del Complejo Volcánico Laguna del Maule y su control sobre la deformación cortical, Undergraduate thesis, Concepción: Universidad de Concepción, 225, 2016.

Koper, K. D., Hutko, A. R., Lay, T., and Sufri, O.: Imaging short-period seismic radiation from the 27 February 2010 Chile (M_{w} 8.8) earthquake by back-projection of P, PP, and PKIKP waves, J. Geophys. Res., 117, B02308, https://doi.org/10.1029/2011JB008576, 2012.

Lamb, S. and Davis, P.: Cenozoic climate change as a possible cause for the rise of the Andes, Nature, 425, 792–797, https://doi.org/10.1038/nature02049, 2003.

Lanza, F., Tibaldi, A., Bonali, F. L., and Corazzato, C.: Space–time variations of stresses in the Miocene–Quaternary along the Calama–Olacapato–El Toro Fault Zone, Central Andes, Tectonophysics, 593, 33–56, 2013.

Lara, L., Lavenu, A., Cembrano, J., and Rodríguez, C.: Structural controls of volcanism in transversal chains: resheared faults and neotectonics in the Cordón Caulle–Puyehue area (40.5° S), Southern Andes, J. Volcanol. Geoth. Res., 158, 70–86, https://doi.org/10.1016/j.jvolgeores.2006.04.017, 2006.

Lay, T.: The surge of great earthquakes from 2004 to 2014, Earth Planet. Sc. Lett., 409, 133–146, 2015.

Lay, T. and Bilek, S. L.: Anomalous earthquake ruptures at shallow depths on subduction zone megathrusts, in: The Seismogenic Zone of Subduction Thrust Faults, edited by: Dixon, T. H. and Moore, J. C., Columbia University Press, New York, 476–511, https://doi.org/10.7312/dixo13866-015, 2007.

Lay, T., Kanamori, H., and Ruff, L.: The asperity model and the nature of large subduction zone earthquake occurrence, Earthquake Pred. Res., 1, 3–71, 1982.

Lay, T., C. Ammon, J., Kanamori, H., Koper, K. D., Sufri, O., and Hutko, A. R.: Teleseismic inversion for rupture process of the 27 February 2010 Chile (M_w 8.8) earthquake, Geophys. Res. Lett., 37, L13301, https://doi.org/10.1029/2010GL043379, 2010.

Lay, T., Yue, H. E. E., Brodsky, E. E., and An, C.: The 1 April 2014 Iquique, Chile M_w 8.1 earthquake rupture sequence, Geophys. Res. Lett., 41, 3818–3825, https://doi.org/10.1002/2014GL060238, 2014.

Lee, S. J., Yeh, T. Y., Lin, T. C., Lin, Y. Y., Song, T. R., and Huang, B. S.: Two-stage composite megathrust rupture of the 2015 M_w 8.4 Illapel, Chile, earthquake identified by spectral-element inversion of teleseismic waves, Geophys. Res. Lett., 43, 4979–4985, https://doi.org/10.1002/2016GL068843, 2016.

Leon-Rios, S., Reyes-Wagner, V., Calle-Gardella, D., Rietbrock, A., Roecker, S., Maksymowicz, A., and Comte, D.: Structural characterization of the Taltal segment in northern Chile between 22° S and 26° S using local earthquake tomography, Geochem. Geophy. Geosy., 25, e2023GC011197, https://doi.org/10.1029/2023GC011197, 2024.

Li, L., Lay, T., Cheung, K. F., and Ye, L.: Odellingdeling of teleseismic and tsunami wave observations to constrain the 16 September 2015 Illapel, Chile, M_w 8.3 earthquake rupture process, Geophys. Res. Lett., 43, 4303–4312, https://doi.org/10.1002/2016GL068674, 2016.

Lin, Y. N. N., Sladen, A., Ortega-Culaciati, F., Simons, M., Avouac, J. P., Fielding, E. J., and Socquet, A.: Coseismic and postseismic slip associated with the 2010 Maule Earthquake, Chile: Characterizing the Arauco Peninsula barrier effect, J. Geophys. Res.-Sol. Ea., 118, 3142–3159, 2013.

Lorito, S., Romano, F., Atzori, S., Tong, X., Avallone, A., McCloskey, J., Cocco, M., Boschi, E., and Piatanesi, A.: Limited overlap between the seismic gap and coseismic slip of the great 2010 Chile earthquake, Nat. Geosci., 4, 173–177, https://doi.org/10.1038/ngeo1073, 2011.

Loveless, J. P. and Meade, B. J.: Stress modulation on the San Andreas fault by interseismic fault system interactions, Geology, 39, 1035–1038, https://doi.org/10.1130/G32215.1, 2011.

Lutz, B. M., Axen, G. J., van Wijk, J. W., and Phillips, F. M.: Whole-lithosphere shear during oblique rifting, Geology, 50, 412–416, https://doi.org/10.1130/G49603.1, 2022.

Maekawa, H., Shzui, M., Ishii, T., Freyer, P., and Pearce, J. A.: Blueshist metamorphism in active subduction zone, Nature, 364, 520–523, 1993.

Maksymowicz, A.: The geometry of the Chilean continental wedge: Tectonic segmentation of subduction processes off Chile, Tectonophysics, 659, 183–196, https://doi.org/10.1016/j.tecto.2015.08.007, 2015.

Marrett, R. A., Allmendinger, R. W., Alonso, R. N., and Drake, R. E.: Late Cenozoic tectonic evolution of the Puna Plateau and adjacent foreland, northwestern Argentine Andes, J. S. Am. Earth Sci., 7, 179–207, 1994.

Martínez-Loriente, S., Sallarès, V., Ranero, C. R., Ruh, J. B., Barckhausen, U., Grevemeyer, I., and Bangs, N.: Influence of incoming plate relief on overriding plate deformation and earthquake nucleation: Cocos Ridge subduction (Costa Rica), Tectonics, 38, 4360–4377, https://doi.org/10.1029/2019TC005586, 2019.

Mccaffrey, R., Stein, S., and Freymueller, J.: Crustal block rotations and plate coupling, Geodynamics, 30, 101–122, 2002.

McCuaig, T. C. and Hronsky, J. M. A.: The mineral system concept: the key to exploration targeting, Soc. Econ. Geol. Spec. P., 18, 153–176, 2014.

Melgar, D., Fan, W., Riquelme, S., Gengm, J., Liang, C., Fuentes, M., Vargas, G., Allen, R. M., Shearer, P. M., and Fielding, E. J.: Slip segmentation and slow rupture to the trench during the 2015, M_w 8.3 Illapel, Chile earthquake, Geophys. Res. Lett., 43, 961–966, https://doi.org/10.1002/2015GL067369, 2016.

Melnick, D. and Echtler, H. P.: Morphotectonic and Geological digital Map Compilations of the South-Central Chile (36°–42° S), in: The Andes active subduction orogeny, Onken, O., Chong, G., Franz, G., Giese, P., Götze, H., Ramos, V. A., Strecker, M. R., and Wigger, P., Frontiers in Earth Sciences, 565–568, Elsevier, 569 pp., 2006.

Melnick, D., Bookhagen, B., Strecker, M., and Echtler, H.: Segmentation of megathrust rupture zones from fore-arc deformation patterns over hundreds to millions of years, Arauco Peninsula, Chile, J. Geophys. Res., 114, 0148–0227, https://doi.org/10.1029/2008JB005788, 2009.

Menant, A., Angiboust, S., Gerya, T., Lacassin, R., Simoes, M., and Grandin, R.: Transient stripping of subducting slabs controls periodic forearc uplift, Nat. Commun., 11, 1823, https://doi.org/10.1038/s41467-020-15580-7, 2020.

Mendoza, C., Hartzel, S., and Monfret, T.: Wide-band analysis of the 3 March 1985 central Chile earthquake: Overall source process and rupture history, B. Seismol. Soc. Am., 84, 269–283, 1994.

Métois, M., Socquet, A., and Vigny, C.: Interseismic coupling, segmentation and mechanical behavior of the Central Chile subduction zone, J. Geophys. Res., 117, https://doi.org/10.1029/2011JB008736, 2012.

Métois, M., Vigny, C., and Socquet, A.: Interseismic Coupling, megathrust earthquakes and seismic swarms along the Chilean Subduction Zone (38°–18° S), Pure Appl. Geophys., 173, 1431–1449, https://doi.org/10.1007/s00024-016-1280-5, 2016.

Miller, N. C., Lizarralde, D., Collins, J. A., Holbrook, W. S., and Van Avendonk, H. J.: Limited mantle hydration by bending faults at the Middle America Trench, J. Geophys. Res.-Sol. Ea., 126, e2020JB020982, https://doi.org/10.1029/2020JB020982, 2021.

Mogi, K.: Earthquake Prediction, Academic Press, Tokyo, 1985.

Molina, D., Tassara, A., Abarca, R., Melnick, R. D., and Madella, A.: Frictional segmentation of the Chilean megathrust from a multivariate analysis of geophysical, geological, and geodetic data, J. Geophys. Res.-Sol. Ea., 126, e2020JB020647, https://doi.org/10.1029/2020JB020647, 2021.

Moreno, M., Rosenau, M., and Oncken, O.: 2010 Maule earthquake slip correlates with pre-seismic locking of Andean subduction zone, Nature, 467, 198–202, https://doi.org/10.1038/nature09349, 2010.

Moreno, M., Melnick, D., Rosenau, M., Baez, J., Klotz J., Oncken, O., Tassara, A., Chen, J., Bataille, K., Bevis, M., Socquet, A., Bolte, J., Vigny, C., Brooks, B., Ryder, I., Grund, V., Smalley, B., Carrizo, D., Bartsch, M., and Hase, H.: Toward understanding tectonic control on the M_w 8.8 2010 Maule Chile earthquake, Earth Planet. Sc. Lett., 321, 152–165, 2012.

Moreno, M., Haberland, C., Oncken, O., Rietbrock, A., Angiboust, S., and Heidbach, O.: Locking of the Chile subduction zone controlled by fluid pressure before the 2010 earthquake, Nat. Geosci., 7, 292–296, 2014.

Moscoso, E. and Grevemeyer, I.: Bending-related faulting of the incoming oceanic plate and its effect on lithospheric hydration and seismicity: A passive and active seismological study offshore Maule, Chile, J. Geodyn., 90, 58–70, https://doi.org/10.1016/j.jog.2015.06.007, 2015.

Mpodozis, C. and Ramos, V.: The andes of Chile and Argentina, in: Geology of the Andes and its relation to hydrocarbon and mineral resources:Houston, Texas, Circum-Pacific Council for Energy and Mineral Resources Earth Science Series. Circum Pacific Council Publications, edited by: Ericksen, G. E., Canas-Pinochet, M. T., and Reinemund, J. A., v. 11, chapter 5, 59–90, 1990.

Müller, R. D., Zahirovic, S., Williams, S. E., Cannon, J., Seton, M., Bower, D. J., Tetley, M. G., Heine, C., Le Breton, E., Liu, S., Russell, S. H. J., Yang, T., Leonard, J., and Gurnis, M.: A global plate model including lithospheric deformation along major rifts and orogens since the Triassic, Tectonics, 38, 1884–1907, https://doi.org/10.1029/2018TC005462, 2019.

Nealy, J. L., Herman, M. W., Moore, G. L., Hayes, G. P., Benz, H. M., Bergman, E. A., and Barrientos, S. E.: 2017 Valparaíso earthquake sequence and the megathrust patchwork of central Chile, Geophys. Res. Lett., 44, 8865–8872, https://doi.org/10.1002/2017GL074767, 2017.

Niemeyer, H., Berrios, H., and de la Cruz, R.: Temperatures of formation in Triassic cataclasites of Cordillera Domeyko, Antofagasta, Chile, Rev. Geol. Chile, 31, 3–18, 2004.

NOAA National Centers for Environmental Information: ETOPO 2022 15 Arc-Second Global Relief Model, NOAA National Centers for Environmental Information [data set], https://doi.org/10.25921/fd45-gt74, 2022.

Okada, Y.: Surface Deformation due to Shear and Tensile Faults in a Half-Space, B. Seismol. Soc. Am., 75, 1135–1154, 1985.

Palacios, C., Ramírez, L. A., Townley, B., Solari, M., and Guerra, N.: The role of the Antofagasta–Calama Lineament in ore deposit deformation in the Andes of northern Chile, Miner. Deposita, 42, 301–308, 2007.

Pasten-Araya, F., Salazar, P., Ruiz, S., Rivera, E., Potin, B., Maksymowicz, A., Torres, E., Villarroel, J., Cruz, E., Valenzuela, J., Jaldín, D., González, G., Bloch, W., Wigger, P., and Shapiro, S. A.: Fluids along the plate interface influencing the frictional regime of the Chilean subduction zone, northern Chile, Geophys. Res. Lett., 45, 10378–10388, https://doi.org/10.1029/2018GL079283, 2018.

Peacock, S. M.: Large-scale hydration of the lithosphere above subducting slabs, Chem. Geol., 108, 49–59, https://doi.org/10.1016/0009-2541(93)90317-C, 1993.

Pearce, R. K., Sánchez de la Muela, A., Moorkamp, M., Hammond, J. O. S., Mitchell, T. M., Cembrano, J. Araya-Vargas, J., Meredith, P. G., Iturrieta, P., Pérez-Estay, N., Marshall, N. R., Smith, J., Yañez, G., Griffith, A., Marquardt, C., Stanton-Yonge, A., and Núñez, R.: Reactivation of fault systems by compartmentalized hydrothermal fluids in the Southern Andes revealed by magnetotelluric and seismic data, Tectonics, 39, e2019TC005997, https://doi.org/10.1029/2019TC005997, 2020.

Peña, M.: Origen de las Rotaciones Tectónicas en el Márgen Occidental de América del Sur: Influencia de Heterogeneidades en las Placas de Nazca y Sudamericana, Tesis para Optar al Grado de Doctor en Ciencias, Mencion Geología, Inédito, 214 p., Universidad de Chile, Facultad de Ciencias Físicas Y Matemáticas, Departamento de Geología, Chile, unplublished thesis, 2022.

Perrin, C., Waldhauser, F., and Scholz, C. H.: The shear deformation zone and the smoothing of faults with displacement, J. Geophys. Res.-Sol. Ea., 126, e2020JB020447, https://doi.org/10.1029/2020JB020447, 2021.

Philibosian, B. and Meltzner, A. J.: Segmentation and supercycles: A catalog of earthquake rupture patterns from the Sumatran Sunda Megathrust and other well-studied faults worldwide, Quaternary Sci. Rev., 241, 106390, https://doi.org/10.1016/j.quascirev.2020.106390, 2020.

Piquer, J., Skármeta, J., and Cooke, D. R.: Structural evolution of the Río Blanco-Los Bronces district, Andes of central Chile: controls on stratigraphy, magmatism and mineralization, Econ. Geol., 110, 1995–2023, 2015.

Piquer, J., Berry, R. F., Scott, R. J., and Cooke, D. R.: Arc-oblique fault systems: their role in the Cenozoic structural evolution and metallogenesis of the Andes of central Chile, J. Struct. Geol., 89, 101–117, https://doi.org/10.1016/j.jsg.2016.05.008, 2016.

Piquer, J., Yáñez, G., Rivera, O., and Cooke, D. R.: Long-lived damage zones associated with fault intersections in the Andes of Central Chile, Andean Geol., 46, 223–239, https://doi.org/10.5027/andgeoV46n2-3106, 2019.

Piquer, J., Rivera, O., Yáñez, G., and Oyarzún, N.: The Piuquencillo fault system: a long-lived, Andean-transverse fault system and its relationship with magmatic and hydrothermal activity, Solid Earth, 12, 253–273, https://doi.org/10.5194/se-12-253-2021, 2021a.

Piquer, J., Sanchez-Alfaro, P., and Pérez-Flores, P.: A new model for the optimal structural context for giant porphyry copper deposit formation, Geology, 49, 597–601, https://doi.org/10.1130/G48287.1, 2021b.

Platt, J. P., Xia, H., and Schmidt, W. L.: Rheology and stress in subduction zones around the asesimic/sesimic transition, Prog. Earth Planet. Sci. 5, 24, https://doi.org/10.1186/s40645-018-0183-8, 2018.

Poli, P., Maksymowicz, A., and Ruiz, S.: The M_{w} 8.3 Illapel earthquake (Chile): Preseismic and postseismic activity associated with hydrated slab structures, Geology, 45, 247–250, https://doi.org/10.1130/G38522.1, 2017.

Pritchard, M. E., Simons, M., Rosen, P. A., Hensley, S., and Webb, F. H.: Co-seismic slip from the 1995 July 30 $M_{\mathrm{w}} =$ 8.1 Antofagasta, Chile, earthquake as constrained by InSAR and GPS observations, Geophys. J. Int., 150, 362–376, https://doi.org/10.1046/j.1365-246X.2002.01661.x, 2002.

Radic, J. P.: Las cuencas cenozoicas y su control en el volcanismo de los Complejos Nevados de Chillán y Copahue-Callaqui (Andes del Sur, 36–39° S), Andean Geol., 37, 220–246, https://doi.org/10.5027/andgeoV37n1-a09, 2010.

Ramos, V.: The Basement of Central Andes: The Arequipa and Related Terranes, Annu. Rev. Earth Pl. Sc., 36, 289–324, 2008.

Ramos, V. and Kay, S.: Overview of the tectonic evolution of southern central Andes of Mendoza and Neuquén (35°–39° S latitude), Geol. Soc. Am. Spec. Pap., 407, 1–18, https://doi.org/10.1130/2006.2407(01), 2006.

Ranero, C. and Sallares, V.: Geophysical evidence for hydration of the crust and mantle of the Nazca plate during bending at the north Chile Trench, Geology, 32, 549–552, https://doi.org/10.1130/G20379.1, 2004.

Ranero, C. R., Villaseñor, A., Phipps Morgan, J., and Weinrebe, W.: Relationship between bend-faulting at trenches and intermediate-depth seismicity, Geochem. Geophy. Geosy., 6, Q12002, https://doi.org/10.1029/2005GC000997, 2005.

Ranero, C. R., Grevemeyer, I., Sahling, H., Barckhausen, U., Hensen, C., Wallmann, K., Weinrebe, W., Vannucchi, P., von Huene, R., and McIntosh, K.: Hydrogeological system of erosional convergent margins and its influence on tectonics and interplate seismogenesis, Geochem. Geophy. Geosy., 9, Q03S04, https://doi.org/10.1029/2007GC001679, 2008.

Richards, J. P., Jourdan, F., Creaser, R. A., Maldonado, G., and DuFrane, S. A.: Geology, geochemistry, geochronology, and economic potential of Neogene volcanic rocks in the Laguna Pedernal and Salar de Aguas Calientes segments of the Archibarca lineament, northwest Argentina, J. Volcanol. Geoth. Res., 258, 47–73, 2013.

Rivera, O.: Geodynamic Setting for Porphyry Copper Deposits in Central Chile: Role of Translithospheric Structures and Gravimetric Anomalies in Andean Metallogeny, Master Thesis, Department of Geological Sciences, Faculty of Engineering and Geological Sciences, Catholic University of the North, Chile, 215 pp., 2017.

Rivera, O., and Cembrano, J.: Modelo de Formación de Cuencas Volcano-Tectónicas en Zonas de Transferencia Oblicuas a la Cadena Andina: El Caso de las Cuencas Oligo-Miocenas de Chile Central y su Relación con Estructuras WNW-NW (33º00'–34º30' LS), in: 9th Congreso Geológico Chileno, Actas, vol. Nº2, 631–636, Puerto Varas-Chile, 2000.

Roland, E. and McGuire, J. J.: Earthquake swarms on transform faults, Geophys. J. Int., 178, 1677–1690, https://doi.org/10.1111/j.1365-246X.2009.04214.x, 2009.

Roquer, T., Arancibia, G., Rowland, J., Iturrieta, P., Morata, D., and Cembrano, J.: Fault-controlled development of shallow hydrothermal systems: structural and mineralogical insights from the Southern Andes, Geothermics, 66, 156–173, https://doi.org/10.1016/j.geothermics.2016.12.003, 2017.

Ruegg, J. C., Campos, J., Armijo, R., Barrientos, S., Briole, P., Thiele, R., Arancibia, M., Cañuta, J., Duquesnoy, T., Chang, M., Lazo, D., Lyon-Caen, H., Ortlieb, L., Rossignol, J. C., and Serrurier, L.: The $M_w = 8.1$ Antofagasta earthquake of July 30 1995: first results from teleseismic and geodetic data, Geophys. Res. Lett., 23, 917–920, 1996.

Ruepke, L., Morgan, J., Hort, M., and Connolly, J.: Serpentine and the subduction water cycle, Earth Planet. Sc. Lett., 223, 17–34, https://doi.org/10.1016/j.epsl.2004.04.018, 2004.

Ruiz, S. and Madariaga, R.: Historical and recent large megathrust earthquakes in Chile, Tectonophysics, 1733, 37–56, https://doi.org/10.1016/j.tecto.2018.01.015, 2018.

Ruiz, S., Madariaga, R., Astroza, M., Saragoni, G. R., Lancieri, M., Vigny, C., and Campos, J.: Short Period Rupture Process of the 2010 M_w 8.8 Maule Earthquake in Chile, Earthq. Spectra, 28, S1–S18, 2012.

Ruiz, S., Metois, M., Fuenzalida, A., Ruiz, J., Leyton, F., Grandin, R., Vigny, C., Madariaga, R., and Campos, J.: Intense foreshocks and a slow slip event preceded the 2014 Iquique M_w 8.1 earthquake, Science, 345, 1165–1169, https://doi.org/10.1126/science.1256074, 2014.

Saffer, D. M.: Mapping fuids to subduction megathrust locking and slip behavior: Fluids and Subduction Megathrust Locking, Geophys. Res. Lett., 44, 9337–9340, 2017.

Saffer, D. M. and Tobin, H.: Hydrogeology and Mechanics of Subduction Zone Forearcs: Fluid Flow and Pore Pressure, Annu. Rev. Earth Pl. Sc., 39, 157–186, https://doi.org/10.1146/annurev-earth-040610-133408, 2011.

Sagripanti, L., Folguera, A., Gimenez, M., Rojas Vera, E. A., Fabiano, J. J., Molnar, N., Fennell, L., and Ramos, V. A.: Geometry of Middle to Late Triassic extensional deformation pattern in the Cordillera del Viento (Southern Central Andes): a combined field and geophysical study, J. Iber. Geol., 40, 349–366, 2014.

Saillard, M., Audin, L., Rousset, B., Avouac, J. P., Chlieh, M., Hall, S. R., Husson, L., and Farber, D. L.: From the seismic cycle to long-term deformation: linking seismic coupling and Quaternary coastal geomorphology along the Andean megathrust, Tectonics, 36, 241–256, https://doi.org/10.1002/2016TC004156, 2017.

Salfity, J. A.: Lineamentos transversales al rumbo andino en el Noroeste Argentino, in: IV Congreso Geológico Chileno, Antofagasta, Chile, vol. 2, 119–137, 1985.

Santibáñez, I., Cembrano, J., García-Pérez, T., Costa, C., Yáñez, G., Marquardt, C., Arancibia, G., and González, G.: Crustal faults in the Chilean Andes: geological constraints and seismic potential, Andean Geol., 46, 32–65, https://doi.org/10.5027/andgeoV46n1-3067, 2019.

Satake, K. and Heidarzadeh, M.: A Review of Source Models of the 2015 Illapel, Chile Earthquake and Insights from Tsunami Data, in: The Chile-2015 (Illapel) Earthquake and Tsunami, Pageoph Topical Volumes, edited by: Braitenberg, C. and Rabinovich, A., Birkhäuser, Cham, https://doi.org/10.1007/978-3-319-57822-4_1, 2017.

Scholz, C. H.: The Mechanics of Earthquakes and Faulting, 2nd edn., Cambridge University Press, 504 pp., ISBN 052165235, 1990.

Scholz, C. H. and Campos, J.: The seismic coupling of subduction zones revisited, J. Geophys. Res., 117, B05310, https://doi.org/10.1029/2011JB009003, 2012.

Schurr, B., Asch, G., Rosenau, M., Wang, R., Oncken, O., Barrientos, S., Salazar, P., and Vilotte, J. P.: The 2007 M 7.7 Tocopilla northern Chile earthquake sequence: Implications for along-strike and downdip rupture segmentation and megathrust frictional behavior, J. Geophys. Res., 117, B05305, https://doi.org/10.1029/2011JB009030, 2012.

Schurr, B., Asch, G., Hainzl, S., Edford, J., Hoechner, A., Palo, M., Wang, R., Moreno, M., Bartsch, M., Zhang, Y., Oncken, O., Tilmann, F., Dahm, T., Victor, P., Barrientos, S., and Vilotte, J.-P.: Gradual unlocking of plate boundary controlled initiation of the 2014 Iquique earthquake, Nature, 512, 299–302, https://doi.org/10.1038/nature13681, 2014.

SERNAGEOMIN: Mapa Geológico de Chile 1 : 1 000 000: digital versión, Servicio Nacional de Geología y Minería, Digital Geological Publication No. 4 (CD-ROM, version 1.0), Santiago, Chile, 2003.

Shillington, D., Bécel, A., Nedimović, M., Kuehn, H., Webb, S., Abers, G., Keranen, K., Li, J., Delescluse, M., and Mattei-Salicrup, G.: Link between plate fabric, hydration and subduction zone seismicity in Alaska, Nat. Geosci., 8, 961–964, https://doi.org/10.1038/ngeo2586, 2015.

Sibson, R. H.: Conditions for fault-valve behavior, in: Deformation Mechanisms, Rheology and Tectonics, edited by: Knipe, R. J. and Rutter, E. H., Geological Society [London] Special Publication, 54, 15–28, https://doi.org/10.1144/GSL.SP.1990.054.01.02, 1990.

Sibson, R. H.: Preparation zones for large crustal earthquakes consequent on fault-valve action, Earth Planets Space, 72, 31, https://doi.org/10.1186/s40623-020-01153-x, 2020.

Sielfeld, G., Lange D., and Cembrano, J.: Intra-Arc Crustal Seismicity: Seismotectonic Implications for the Southern Andes Volcanic Zone, Chile, Tectonics, 38, 552–578, https://doi.org/10.1029/2018TC004985, 2019.

Stanton-Yonge, A., Griffith, W. A., Cembrano, J., St. Julien, R., and Iturrieta, P.: Tectonic role of margin-parallel and margin-transverse faults during oblique subduction in the Southern Volcanic Zone of the Andes: Insights from boundary element modelling, Tectonics, 35, 1990–2013, https://doi.org/10.1002/2016TC004226, 2016.

Talwani, P.: Intraplate Earthquakes, Cambridge University press, 360 pp., ISBN-10 1107040388, 2014.

Thingbaijam, K. K. S., Mai, P. M., and Goda, K.: New Empirical Earthquake Source-Scaling Laws, B. Seismol. Soc. Am., 107, 2225–2246, https://doi.org/10.1785/0120170017, 2017.

Torres, J.: Caracterización del lineamiento Laguna fea-volcán san Pedro, región del Maule: Relación con actividad magmática e hidrotermal, Undergraduate thesis, Universidad Austral de Chile, Valdivia, 174, 2021.

Tsuji, T., Ashi, J., and Ikeda, Y.: Strike-slip motion of a mega-splay fault system in the Nankai oblique subduction zone, Earth Planets Space, 66, 120, https://doi.org/10.1186/1880-5981-66-120, 2014.

Vigny, C., Socquet, A., Peyrat, S., Ruegg, J. C., Métois, M., Madariaga, R., Morvan, S., Lancieri, M., Lacassin, R., Campos, J., Carrizo, D., Bejar-Pizarro, M., Barrientos, S., Armijo, R., Aranda, C., Valderas-Bermejo, M.-C., Ortega, I., Bondoux, F., Baize, S., Lyon-Caen, H., Pavez, A., Vilotte, J. P., Bevis, M., Brooks, B., Smalley, R., Parra, H., Baez, J.-C., Blanco, M., Cimbaro, S., and Kendrick, E.: The 2010 M_w 8.8 Maule Megathrust Earthquake of Central Chile, Monitored by GPS, Science, 332, 1417–1421, https://doi.org/10.1126/science.1204132, 2011.

Wall, R., Gana, P., and Gutiérrez, A.: Mapa Geológico del Área de San Antonio-Melipilla, Regiones de Valparaíso, Metropolitana y del Libertador Bernardo O'Higgins, Mapas Geológicos No. 2, Escala 1 : 100 000, Sernageomin, Chile, ISNN 0717-2532, 1996.

Wall, R., Sellés, D., and Gana, P.: Geología del Área Tiltil-Santiago, Región Metropolitana de Santiago, Serie Mapas Geológicos No. 11, Escala 1 : 100 000, Sernageomin, Chile, ISSN 0717-2532, 1999.

Wallace, L. M., Beavan, J., McCaffrey, R., and Darby, D.: Subduction zone coupling and tectonic block rotations in the North Island, New Zealand, J. Geophys. Res., 109, B12406, https://doi.org/10.1029/2004JB003241, 2004.

Wang, K. and Bilek, S. L.: Do subducting seamounts generate or stop large earthquakes?, Geology, 39, 819–822, 2011.

Wdowinski, S.: Dynamically supported trench topography, J. Geophys. Res., 97, 17651–17656, https://doi.org/10.1029/92JB01337, 1992.

Wiemer, D., Hagemann, S. G., Hayward, N., Begg, G. C., Hronsky, J., Thébaud, N., Kemp, A. I. S., and Villanes, C.: Cryptic trans-lithospheric fault systems at the western margin of South America: implications for the formation and localization of gold-rich deposit superclusters, Front. Earth Sci., 11, 1159430, https://doi.org/10.3389/feart.2023.1159430, 2023.

Xia, S., Sun, J., and Huang, H.: Degree of serpentinization in the forearc mantle wedge of Kyushu subduction zone: quantitative evaluations from seismic velocity, Mar. Geophys. Res., 36, 101–112, 2015.

Yañez, G. and Cembrano, J.: The role of the viscous plate coupling in the late tertiary Andean deformation, J. Geophys. Res., 106, 6325–6345, 2004.

Yañez, G. and Rivera, O.: Crustal dense blocks in the forearc and arc region of Chilean ranges and their role in the magma ascent and composition, Breaking paradigms in the Andean metallogeny, J. S. Am. Earth Sci., 93, 51–66, https://doi.org/10.1016/j.jsames.2019.04.006, 2019.

Yañez, G., Gana, P., and Fernández, R.: Sobre el orígen y significado geológico de la anomalía Melipilla, zona central de Chile, Rev. Geol. Chile, 25, 175–198, 1998.

Yañez, G., Ranero, C. R., Von Huene, R., and Díaz, J.: Magnetic anomaly interpretation across the southern central Andes (32°–34° S): The role of the Juan Fernandez Ridge in the late Tertiary evolution of the margin, J. Geophys. Res., 106, 6325–6345, 2001.

Yáñez-Cuadra, V., Ortega-Culaciati, F., Moreno, M., Tassara, A., Krumm-Nualart, N., Ruiz, J., Maksymowicz, A., Manea, M., Manea, V. C., Geng, J., and Benavente, R.: Interplate coupling and seismic potential in the Atacama Seismic Gap (Chile): Dismissing a rigid Andean sliver, Geophys. Res. Lett., 49, e2022GL098257, https://doi.org/10.1029/2022GL098257, 2022.

Yue, L. T., Brodsky, E., and An, C.: The 1 April 2014 Iquique, Chile, M_w 8.1 earthquake rupture sequence, Geophys. Res. Lett., 41, 3818–3825, https://doi.org/10.1002/2014GL060238, 2014.